CAMK1D triggers immune resistance of human PD-L1 refractory tumor cells after cytotoxic T cell attack

Valentina Volpin,[1,2] Tillmann Michels,[1,2] Antonio Sorrentino[1,2], Ayse Nur Menevse[1], Gertrud Knoll[3], Madlen Ditz[1], Vladimir Milija Milenkovic[4], Chih-Yeh Chen[1], Anchana Rathinasamy[1], Klaus Griewank[5], Michael Boutros[6], Sebastian Haferkamp[7], Mark Berneburg[7], Christian Wetzel[4], Anja Seckinger[8], Dirk Hose[8], Hartmut Goldschmidt[9], Martin Ehrenschwender[3], Mathias Witzens-Harig[10], Arpad Szoor[11], Gyorgy Vereb[11], Nisit Khandelwal[12] and Philipp Beckhove[1,2,13]

Affiliations

[1]Regensburg Center for Interventional Immunology (RCI), University Regensburg, Regensburg, 93053, Germany

[2]German Cancer Research Center (DKFZ), Translational Immunology, Heidelberg, 69120, Germany

[3]Institute of Clinical Microbiology and Hygiene, University Hospital Regensburg, 93053, Germany

[4]Department of Psychiatry and Psychotherapy, Molecular Neurosciences, University of Regensburg, 93053 Regensburg, Germany

[5]Department of Dermatology, University Hospital Essen, West German Cancer Center, University Duisburg-Essen and the German Cancer Consortium, Essen, Germany

[6]German Cancer Research Center (DKFZ), Division Signalling and Functional Genomics, Heidelberg, 69120, Germany

[7]Department of Dermatology, University Hospital Regensburg, Regensburg, 93053, Germany

[8]Labor für Myelomforschung, Medizinische Klinik V, Universitätsklinikum Heidelberg, 69120 Heidelberg, Germany

[9]Department of Internal Medicine V and National Center of Tumor Diseases (NCT), University Hospital Heidelberg, 69120 Heidelberg, Germany

[10]Department of Hematology, Oncology and Rheumatology, University Hospital Heidelberg, 69120 Heidelberg, Germany

[11]Department of Biophysics and Cell Biology, Faculty of Medicine, University of Debrecen, 4032 Debrecen Hungary

[12] iOmx Therapeutics AG, 82152 Martinsried/Munich, Germany

[13]Department of Hematology, Oncology, Internal Medicine 3. University Hospital Regensburg, Regensburg, 93053, Germany

Running title

CAMK1D triggers immune resistance inhibiting caspase-3,-6,-7

Funding

This project was funded by the Deutsche Forschungsgemeinschaft (DFG, German Research Foundation) - Projektnummer 324392634 - TRR 221 and the National Research, Development and Innovation Office, Hungary - OTKA K119690.

Correspondence to: Philipp Beckhove, Regensburg Center for Interventional Immunology University Regensburg, Franz-Josef-Strauss-Allee 11, D-93053 Regensburg, Phone: +49-941-944 38101, Email: beckhove@rcii.de

Competing interests: The authors declare no potential conflicts of interest.

Abstract

Success of cancer immunotherapy is limited by resistance against immune-checkpoint blockade. We therefore conducted a genetic screen to identify genes that mediate resistance against cytotoxic T lymphocytes (CTL) in PD-L1 refractory human tumors. Using PD-L1 positive multiple myeloma cells and tumor-reactive marrow-infiltrating CTL as a model we identified calcium/calmodulin-dependent protein kinase 1D (CAMK1D) as a key modulator of tumor intrinsic immune resistance. CAMK1D was co-expressed with PD-L1 in PD-L1/PD-1 refractory cancer types and correlated with poor prognosis in these tumors. CAMK1D was activated by CTL through Fas-receptor stimulation, which induced its binding to and phosphorylation of all effector caspases -3, -6 and -7, thereby inhibiting their activation and function. Consistently, CAMK1D mediated immune resistance of murine colorectal cancer cells *in vivo*. The pharmacological inhibition of CAMK1D on the other hand, restored the sensitivity towards Fas-ligand treatment in multiple myeloma as well as in uveal melanoma cells *in vitro*. Thus, we report a mechanism of rapid inhibition of the terminal apoptotic cascade by a kinase expressed in PD-L1 refractory tumors that can be tuned through T cell activity and may contribute to tumor immune resistance upon immune-checkpoint blockade.

Synopsis

We here report a novel mechanism of profound T cell induced apoptosis resistance and conclude that CAMK1D may represent an important immune escape mechanism triggered upon T cell attack in PD-L1 treatment refractory tumors.

Introduction

Endogenous T cell responses against tumor antigens occur frequently in a broad variety of cancer types (1-3). Although these can correlate with an overall improvement of patient prognosis (2, 4, 5), they often do not rescue patients from tumor progression. A major reason for the inability of tumor-reactive cytotoxic T cells to eradicate established tumors lies in the capacity of tumor cells to regulate T cell activity through expression of the immune-inhibitory ligand PD-L1, which stimulates the inhibitory receptor PD-1 expressed on effector T cells and reduces T cell receptor signaling. PD-L1 expression in healthy and tumor tissues is itself induced by effector T cell activity through the secretion of inflammatory cytokines such as IFN-gamma (6-8) and serves as an important mechanism to prevent autoimmune diseases. Consequently, blockade of PD-L1/PD-1 interactions by therapeutic antibodies has resulted in stunning immune rejection of established, even metastasized tumors in many patients with PD-L1 expressing tumors (9-12).

However, despite noteworthy improvements, a significant proportion of cancer patients lack response to anti-PD-L1/PD-1 antibody therapies (13-15). Several mechanisms of PD-L1/PD-1 treatment resistance have been recently introduced including impaired tumor intrinsic IFN-gamma responsiveness resulting in reduced PD-L1 expression, severe and irreversible T cell exhaustion or block of T cell differentiation induced by chronic PD-1 over-stimulation (16). However, since functional capacity of tumor reactive T cells is found in many patients with PD-L1/PD-1 refractory tumors (3, 5), these mechanisms may only explain immune response resistance in a minor fraction of cases. Therefore, additional immune regulatory interactions may impose dominant levels of protection against immune destruction. Indeed, several immune inhibitory receptors such as TIM3 or VISTA, which can be triggered by ligands expressed in tumors, have been characterized in the past (17, 18). Nevertheless, it is well conceivable that

immune resistance is not only conveyed by immune regulatory ligands controlling T cell activity, but may also be achieved by tumor intrinsic mechanisms of resistance against the cytotoxic T cell attack.

Here, we report on a systematic search for genes regulating immune responsiveness in tumor cells, using multiple myeloma as a PD-L1 expressing human tumor model that is unresponsive towards anti-PD-L1/PD-1 treatment.

Multiple myeloma (MM) is still a rarely curable B-cell malignancy characterized by the accumulation of malignant plasma cell clones in the bone marrow. In MM spontaneous cytotoxic T cell responses against myeloma-associated antigens occur (1). Several studies showed that immune-checkpoint molecules are expressed by myeloma cells and induce tumor-related immune suppression (19-21). In line, PD-L1 is commonly expressed on malignant plasma cells (8) and high expression of PD-L1 is associated with disease progression and has been found further upregulated at relapse or in the refractory stage (22). Still, preliminary results of a phase I trial with PD-1 blocking antibodies were disappointing, reporting no objective responses amongst the 27 treated multiple myeloma patients (23). Therefore, there is a rationale to assume that other immune-checkpoint molecules may play a crucial role in tumor escape mechanisms in this tumor entity. This is of special relevance as immunotherapeutic treatment options emerge in multiple myeloma, including monoclonal antibodies against CD38 (e.g. daratumumab, isatuximab), SLAMF7 (elotuzumab), BCMA-CAR-T-based treatments or BCMA-T-cell bispecific antibodies (24-28).

In order to systematically identify genes that inhibit tumor immune destruction by cytotoxic T cells, we applied a high-throughput (HTP) genetic screen allowing the silencing of a multitude of genes in human multiple myeloma cells, as well as the assessment of subsequent tumor lysis by

117 patient-derived marrow-infiltrating lymphocytes (MILs). We identified 90 genes that regulate
118 immune responsiveness after cytotoxic T cell attack. Among them, Calcium/Calmodulin
119 Dependent Protein Kinase 1D (CAMK1D) was co-expressed with PD-L1 and played a key role
120 in protection against T cell-induced tumor cell killing as well as in patient prognosis, not only in
121 multiple myeloma but also in other PD-L1 refractory human cancer types.
122

Materials and Methods

Experimental model and subject details: Patients, healthy donors, and samples

Patients presenting with previously untreated multiple myeloma (n=332) or monoclonal gammopathy of unknown significance (MGUS; n=22) at the University Hospitals of Heidelberg and Montpellier as well as 10 healthy normal donors have been included in the study approved by the ethics committee (#229/2003 and S-152/2010) after written informed consent. Patients were diagnosed, staged and response to treatment assessed according to standard criteria (29-31).

Samples: Normal bone marrow plasma cells and myeloma cells were purified using anti-CD138 microbeads (Miltenyi Biotec, Bergisch Gladbach, Germany) (32, 33). Peripheral $CD27^+$ memory B-cells (n=11) were FACS-sorted as described (34). The human myeloma cell lines U266, RPMI-8226, LP-1, OPM-2, SK-MM-2, AMO-1, JJN-3, NCI-H929, KMS-12-BM, KMS-11, KMS-12-PE, KMS-18, MM1.S, JIM3, KARPAS-620, L363 and ANBL6 were purchased from the German Collection of Microorganisms and Cell Cultures (Braunschweig, Germany) and the American Type Cell Culture (Wesel, Germany), the XG-lines were generated at INSERM U1040 (Montpellier, France) (35). KMM-1 cells were obtained from the National Institutes of Biomedical Innovation, Health and Nutrition (Osaka, Japan). Cell line identity was assessed for proprietary cell lines by DNA-fingerprinting, mycoplasma-contamination excluded by PCR-based assays, and EBV-infection status by clinical routine PCR-based diagnostics. Polyclonal plasmablastic cells (n=10) were generated as published (33, 36, 37). The human uveal melanoma cell line Mel270 was established, characterized and provided by Prof. Griewank (University Hospital Essen) (38). KMM-1-luc cells were generated after transfection with a pEGFP-luc plasmid (provided by Dr. Rudolf Haase, LMU Munich, Germany) and selected for the G418-resistance gene. Lipofectamine LTX was used as transfection reagent according to the

manufacturer´s instructions. Transfected cells were selected for 14 days with G418-containing medium (0.6 mg/mL). KMM-1-luc cells were sorted twice for the expression of GFP by flow cytometry (with 87% and 100% purity, respectively) and cultured in the presence of 0.6 mg/mL G418. Cell sorting was conducted in collaboration with the DKFZ sorting core facility, using the FACSARIA II cell sorter (BD). KMM-1, U266 and Mel270 were cultured under standard conditions in RPMI media supplemented with 10% fetal calf serum, 100 U/ml penicillin G and 100 µg/ml streptomycin at 37 °C in a humidified atmosphere under 5% CO_2.

MILs isolation

Marrow-infiltrating lymphocytes were isolated from the bone marrow of a multiple myeloma patient. Briefly, T cells were isolated from the negative fraction of CD138-sorted bone marrow cells using untouched Human T cells Dynabeads (Invitrogen). Cells were stained for anti-CD3 (Pacific Blue™ anti-human CD3 (Clone OKT3), Biolegend), anti-CD4 (APC/Cy7 mouse anti-human CD4 (Clone RPA-T4), BD Biosciences) and anti-CD8 (Pacific Blue™ mouse anti-human CD8 (Clone RPA-T8), BD Biosciences), tested for HLA-A2 positivity (APC mouse anti-human HLA-A2 Clone BB7.2 (RUO), BD Biosciences) and subsequently expanded using the rapid expansion protocol.

MILs expansion

MILs cultures were ex-vivo expanded using a modified version of the Rapid Expansion Protocol (REP) (39, 40). $2x10^6$ of freshly isolated MILs were diluted to 6 $x10^5$ cell/mL in CLM supplemented with 3000 U/mL rHuIL2 (Novartis Pharma). Cells were incubated in 25 cm^2 tissue culture flask for 48h at 37°C and 5% CO_2. PBMCs from three different buffy coats (at a ratio of

1:1:1) were irradiated with 60 Gy (Gammacell 1000) and used as feeder cells to support MILs expansion. $2x10^6$ MILs were co-incubated with $2x10^8$ feeder cells (in a ratio 1:100) in 400 mL of MIL expansion medium (CLM/AIM-V) with 30 ng/mL OKT3 antibody (Thermo Scientific) and 3000 IU/mL IL-2 for 5 days in a G-Rex 100 cell culture flask. Afterwards, 250 mL of supernatant was changed with 150 mL of fresh media and IL-2 was replenished to keep the concentration at 3000 IU/mL. On day 7, MILs were divided into three G-Rex 100 flasks in a final volume of 250 mL medium each and media was again replenished on day 11. On day 14 of the expansion, MILs were counted and frozen in aliquots of $40x10^6$ cells/mL in freezing media A (60% AB serum and 40% RPMI1640) and B (80% AB serum and 20% DMSO).

Generation of flu-antigen specific $CD8^+$ T cells

For the generation of flu-specific $CD8^+$ T cells (flu TC), PBMCs from HLA-A2 healthy donors were isolated. Total $CD8^+$ T cells were sorted from PBMCs by magnetic separation (Miltenyi) (day 0) and expanded in the presence of A2-matched flu peptide (GILGFVFTL) for 14 days. Irradiated autologous $CD8^-$ fraction was used as feeder cells during the first 7 days of expansion. Afterwards, irradiated T2 cells were used as fresh feeder cells. On day 1 and day 8, 100 IU/mL IL2 (Novartis Pharma) and 5 ng/μL IL15 (R&D Systems) were added to the expansion. The percentage of flu-antigen specific T cells was determined by pentamer staining (GILGFVFTL-APC, ProImmune) on day 7 and 14 via flow cytometry analysis. After antigen-specific expansion, flu TC were sorted by FACS and expanded further for 14 days by using rapid expansion protocol.

PCR and qPCR

Gene expression was measured using end-point PCR. Briefly, total RNA was isolated from cell pellets using the RNeasy Mini kit (Qiagen) according to the manufacturer's guidelines. 1 μg of RNA was reverse transcribed to complementary DNA (cDNA) using the QuantiTect reverse transcription kit (Qiagen) according to the manufacturer's protocol. Synthesized cDNA was amplified using conventional PCR. PCR samples were set up in a 25 μL volume using 2x MyTaq HS Red Mix (Bioline), 500 nM of gene-specific primer mix and 100 ng of template cDNA. The PCR program was set as the following: 95°C for 3 min, 35 cycles of 3 repetitive steps of denaturation (95°C for 30 s), annealing (60°C for 30 s) and extension (72°C for 30 s), and a final step at 72°C for 5 min. PCR products were run on a 2% agarose gel in TAE buffer using a gel electrophoresis system (Thermo Scientific) and DNA bands were visualized using UV light of myECL Imager (Thermo Scientific). Knockdown efficiency of siRNA sequences was measured by quantitative PCR (qPCR). For qPCR, 10 ng of template cDNA, 2x QuantiFast SYBR Green PCR mix (Qiagen) and 300 nM of gene-specific primer mix was used per 20 μL reaction and each sample was prepared in triplicates. Reactions were run using the QuantStudio 3 (Applied Biosystems). Expression of several genes was normalized to the expression of β-actin gene and the analysis was performed using comparative Ct method.

Gene expression profiling using U133 2.0 plus arrays (Affymetrix, Santa Clara, CA, USA) was performed as published (32, 41, 42). Expression data are deposited in ArrayExpress under accession numbers E-MTAB-317.

Survival and correlation analysis using The Cancer Genome Atlas (TCGA)

Transcriptomic normalized RNA-Seq by Expectation-Maximization (RSEM) and clinical data from different tumor entities was downloaded using the TCGA2STAT package for R (43). Log2-normalized expression values were correlated (Person's r) using the ggpubr package for R. Survival curves were generated using survminer package for R. FAS expression was cut at the median to generate Fas high and low sets. Similarly, CAMK1D expression was cut at the median for the Kaplan-Meier survival curves. Significance was calculated using the log-rank test.

Reverse siRNA transfection

Gene knockdown in tumor cells was induced using reverse siRNA transfection with Lipofectamine RNAiMAX (Thermo Scientific). Briefly, 200 µL of 250 nM siRNA solution was added to each well of a 6-well plate. 4 µl of RNAiMAX transfection reagent was diluted in 196 µL of RPMI (Sigma-Aldrich) and incubated for 10 min at room temperature (RT). 400 µL of additional RPMI was added and 600 µL of RNAiMAX mix was given to the siRNA coated wells and incubated for 30 min at RT. 3,5 x 10^5 KMM-1 (WT or luc) cells were resuspended in 1,2 mL of antibiotic-free RPMI culture medium supplemented with 10% FCS, seeded in the siRNA-RNAiMAX containing wells and incubated for 48 h at 37°C, 5% CO_2. Final siRNA concentration was 25 nM in all cases.

Phospho-Protein Isolation

To isolate phosphorylated proteins from cells, tumor cells were pelleted at 0,5 x g for 5 min and washed once with PBS at 4°C. The cell pellets were lysed with one pellet volume of Phosphoplex Lysis Buffer (Merck Millipore) containing protease inhibitor cocktail (Cabliochem,

1:100) and phosphatase inhibitor cocktail (Sigma-Aldrich, 1:100) at 4 °C for 15 min on a rotator. Samples were centrifuged at 17000 g at 4°C for 15 min. Supernatants containing the protein lysates were collected into fresh tubes and quantified using the Pierce BCA Protein Assay Kit (Thermo Scientific) according to the manufacturer's protocol. Proteins were stored at -20 °C.

SDS-PAGE

30 µg of protein lysates were denaturated in 4x NuPAGE LDS Sample Buffer (Thermo Scientific) containing 10% ß-mercaptoethanol (PAN) at 70°C for 10 min. Samples were spun down and separated on NuPAGE 4-12% Bis-Tris Gels (Thermo Scientific) along with PageRuler Prestained Protein Ladder (Thermo Scientific) and run at 115-150 V for 90 min.

Semi-Dry Western Blot

Proteins were transferred from the gel to a PVDF membrane (Millipore) using a semi-dry western blot method. The PVDF blotting membrane (Merck Millipore) was activated in 100% methanol (Merck Millipore) for 1 min and afterwards placed in Transfer Buffer (Thermo Science) until use. Blots were assembled from anode to cathode into the Pierce Power Blot cassette (Thermo Scientific) and run at 24 V for 10 min. Membranes were washed in 1x TBS and then placed in blocking solution (5% BSA / 0.05% TBST) for 2 h. Primary antibodies (anti-CAMK1D (Abcam) 1:20000, anti-caspase-3 (Abcam) 1:750, anti-caspase-6 (Abcam) 1:2000, anti-caspase-7 (Thermo Scientific) 1:1000, anti-caspase-3 (phospho S150) (Abcam) 1:850, anti-caspase-6 (phospho S257) (Abcam) 1:250 and sodium potassium ATPase (Abcam) 1:20000) were diluted in 5% BSA / 0.05% TBST and kept on the membrane overnight at 4°C on a rotator. Membranes were then washed three times for 10 min with 1 % BSA / 0.05% TBST. Afterwards,

HRP-conjugated secondary antibodies (anti-rabbit 1:4000, Santa Cruz or anti-mouse 1:4000, Santa Cruz) were added to 1% BSA/TBST and kept on the membrane at room temperature for 1h on a shaker. Thereafter, the membranes were washed for 10 min with 1% BSA/TBST, then TBST and lastly with TBS. The blots were incubated with the ECL Detection Reagent (Reagent A and Reagent B, 1:1, GE Healthcare) for 4 min and the chemiluminescence was detected with myECL Imager (Thermo Scientific).

Co-immunoprecipitation assay

For detection of direct protein-protein interaction, co-immunoprecipitation was performed. Briefly, 10 M tumor cells were seeded in 10 cm^2 petri dishes. The next day, cells were stimulated for 4 h with 100 ng/ml rHuFasL (Biolegend). Unstimulated cells were used as negative control. Afterwards, tumor cells were detached, resuspended in ice cold TBS and centrifuged at 400 g for 6 min at 4°C. Supernatant was discarded, cell pellet was resuspended in 1,5 mL TBS and centrifuged at 500 g for 8 min at 4°C. Cell pellet was lysed with 1,5 mL lysis buffer (50 mM Tris-HCl, 150 mM NaCl, 0,5% NP40 or Triton-X) containing protease inhibitor (Roche complete 25x) and kept on a rotator for 1 h at 4°C. Afterwards, cells were centrifuged for 20 min at 20000 g at 4°C. Supernatant was collected and centrifuged for further 5 min at 20000 g at 4°C. Meanwhile, protein-G agarose (Sigma-Aldrich) was washed with 1 mL TBS and centrifuged for 1 min at 12000 g. 1 mL of cell supernatant containing cytoplasmatic proteins was added to 60 µL protein-G agarose, incubated with anti-caspase-3 (1:50) (Cell Signaling), anti-caspase-6 (1:50) (Abcam) or anti-caspase-7 (1:100) (Cell Signaling) antibodies and incubated overnight on a rotator at 4°C. 90 µL of cell lysates were frozen at -20°C. The next day, the immunoprecipitated samples were centrifuged at 12000 g at 4°C for 1 min. Supernatant was discarded and protein-G

agarose was washed three times with lyses buffer and centrifuged at 12000 g at 4°C for 1 min. 2x LDS containing 10% β-mercaptoethanol was added to the immunoprecipitated samples, while 4x LDS containing 10% β-mercaptoethanol was added to the lysates. Samples were denaturated for 10 min at 95°C on a thermocycler. Samples were spun down and separated on NuPAGE 4-12% Bis- Tris Gels (Thermo Scientific) along with PageRuler Prestained Protein Ladder (Thermo Scientific) and run at 115-150 V for 90 min. After electrophoresis, proteins were transferred on a PVDF membrane (Millipore). Anti-CAMK1D antibody (1:10000) was diluted in 5% BSA / 0.05% TBST and kept on the membrane overnight at 4°C on a rotator. Membranes were then washed three times for 10 min with 1% BSA / 0.05% TBST. Afterwards, HRP-conjugated secondary antibodies (anti-rabbit 1:3000) (Santa-Cruz) was added to 1% BSA / TBST and kept on the membrane at room temperature for 1 h on a shaker. The membrane was washed. The blot was incubated with the ECL Detection Reagent (Reagent A and Reagent B, 1:1, GE Healthcare) for 4 min and the chemiluminescence was detected with myECL Imager (Thermo Scientific).

Plasmid transfection

To generate KMM-1-luc cells, 3,5 x 10^5 KMM-1 WT cells were seeded in a 6 well plate and incubated at 37°C overnight. 15 µL Lipofectamine LTX reagent were diluted in 150 µL Opti-MEM medium (Gibco). Simultaneously, 3.5 µg of pEGFP-Luc plasmid was diluted in 175 µL Opti-MEM medium and 3.5 µL of PLUS Reagent was added. 150 µL of diluted DNA was added to 150 µL diluted Lipofectamine LTX (Life Technologies) reagent and incubated for 5 min at RT. DNA-lipid complex was then added to the growth medium of the myeloma cells. Cells were incubated at 37°C for 48 h before investigation of transfection efficacy by flow cytometry.

Luciferase-based cytotoxicity assay

KMM-1-luc cells were reverse transfected with the desired siRNA sequences in white 96-well-plate (Perkin Elmer) and incubated for 48 h at 37°C, 5% CO_2. At the same day of transfection MILs were thawn and treated with benzonase (100 IU/mL) (Merck). Cell density was adjusted to 0,6 x 10^6 cells/mL in CLM supplemented with 3000 IU/mL rhuIL-2 (Novartis) for 48 h. IL-2 was depleted 24 h before the co-culture. Flu TC were thawn 6 h before co-culture. For the cytotoxicity setting, MILs, flu TC, the supernatant of activated MILs or rHuFasL were added to transfected tumor cells at desired E:T ratio/concentration, and incubated for 20 h at 37°C, 5% CO_2. For the viability setting, only CLM was added to the tumor cells. After co-culture, supernatant was removed, remaining tumor cells were lysed using 40 µL/well of cell lysis buffer for 10 min. After tumor cell lysis, 60 µL/well of luciferase assay buffer was added and luciferase intensity was measured by using the Spark 20M plate reader (Tecan) with a counting time of 100 msec. Luciferase activities (relative luminescence units = RLUs) were either represented as raw luciferase values or as normalized data to scramble or unstimulated controls.

Real-time live-cell imaging assay

Target genes in KMM-1 or U266 tumor cells were knocked down with reverse siRNA transfection for 48 h. The reverse siRNA transfection was performed using transparent 96 well microplates (TPP). In parallel, MILs were thawn and prepared as previously described. After 48 h, MILs (E:T 10:1) or rHuFasL (100 ng/mL) were added to the target cells in CLM with YOYO-1 (final concentration 1:5000) and co-cultured at 37°C. For viability controls the according amount of CLM with YOYO-1 (final concentration 1:5000) was added. MILs or rHuFasL-mediated tumor lysis was imaged on the green channel using an IncuCyte ZOOM live cell

imager (ESSEN BioScience) for the indicated time points at a 10x magnification. Data were analyzed with the Incucyte ZOOM 2016A software by creating a top-hat filter-based mask for the calculation of the area of YOYO-1 incorporating cells (indicating dead cells).

ELISA

Tumor cells were transfected with the indicated siRNAs in a 96-well plate. Afterwards, T cells were added at the indicated E:T ratio for 20 h and 100 µL of supernatants were harvested for the detection of IFN-γ (Human IFN-γ ELISA Set; BD OptEIA), IL-2 (Human IL-2 ELISA Set; BD OptEIA), Granzyme B (Human Granzyme B ELISA development kit; Mabtech) and TNF (Human TNF ELISA Set; BD OptEIA). Experiments were performed according to the manufacturer´s instructions. Polyclonal stimulation (Dynabeads Human T-Activator CD3/CD28, Invitrogen) was used as positive control. Absorbance was measured at λ = 450 nm, taking λ = 570 nm as reference wavelength using the Spark microplate reader (TECAN).

Flow cytometry (FACS)

Flow cytometry was used for the detection of proteins expressed on the plasma membrane of tumor and T cells. Intracellular staining was performed for the detection of caspase-3 (FITC Active Caspase-3 Apoptosis Kit, BD Bioscience) according to manufacturer's instruction. Tumor cells were detached from plates using PBS-EDTA, centrifuged at 500 x g for 5 min and resuspended in FACS buffer (5 x 10^5 cells/tube). Live T cell and tumor cells were distinguished by using Live/Dead Fixable Yellow dead Cell Stain (Life Technologies) followed by blocking with kiovig (human plasma-derived immunoglobulin, Baxter, Deerfield, Illinois, USA) at a concentration of 100 µg/mL in FACS buffer (PBS, 2% FCS) for 15 min in the dark on ice.

Samples were washed two times in FACS buffer and incubated with either fluorophore-conjugated primary antibodies or isotype control (APC anti-human CD274 (PD-L1) (Clone 29E.2A3), Biolegend; Alexa Fluor 647 Mouse anti-human CCR9 (Clone 112509 (RUO), BD Biosciences; Brilliant Violet 421 anti-human CD95 (Fas) (Clone DX2), Biolegend; PE anti-human CD95 (Fas) (Clone DX2), Biolegend; APC anti-human CD261 (DR4, TRAIL-R1) (Clone DJR1), Biolegend; PE anti-human CD262 (DR5, TRAIL-R2) (Clone DJR2), Biolegend; Biotin anti-human CD120a (TNFR1) (Clone W15099A), Biolegend; PE/Cy7 anti-human CD120b (TNFR2) (Clone 3G7A02), Biolegend; PE/Cy7 anti-human CD279 (PD-1) Antibody, Biolegend); APC mouse anti-human CD178 (Clone NOK-1), BD Biosciences; PE anti-human CD253 (TRAIL) (Clone RIK2), Biolegend; APC anti-human TNF-α (Clone Mab11), Biolegend for 20 min on ice in the dark. Afterwards, cells were washed twice and acquired with the FACS Canto II cell analyzer machine (BD Bioscience) or FACSLyrics Flow cytometer and data were analyzed using FlowJo (Tree Star).

Calcium Imaging

KMM-1 cells grown on coverslips were washed with Ringer solution (118 mM NaCl, 5 mM KCl, 1.2 mM MgCl2, 1.2 mM Na_2HPO_4 , 2 mM NaH_2PO_4, 1.8 mM CaCl2, 5 mM glucose, 9.1 mM HEPES, pH 7.4, with NaOH) and loaded with Fura-2-AM ester (Thermo Fisher Scientific, Waltham, USA) for 45 min. After 15 min, MILs or rHuFasL (50 ng/ml) was added to scr siRNA transfected cells and recording of the intracellular free Ca^{2+} was continued for further 30 minutes. Experiments were performed using a ZEISS live cell imaging setup based on an inverse microscope (Axio Observer Z.1) equipped with Fluar 40x/1.3 objective lens (ZEISS, Germany). Fura 2-AM-loaded KMM-1 cells were illuminated with light of 340 nm or 380 nm (BP 340/30

HE, BP 387/15 HE) using a fast wavelength switching and excitation device (Lambda DG-4, Sutter Instrument), and fluorescence was detected at 510 nm (BP 510/90 HE and FT 409) using an AxioCam MRm LCD camera (ZEISS). Data were recorded and analyzed with ZEN 2012 software (ZEISS, Jena, Germany).

Generation of supernatants of activated MILs

For the generation of the supernatant of polyclonally activated MILs, 1 x 10^6 MILs were suspended in 1 mL of CLM collected in a 15 mL tube and stimulated with 25 µL of Dynabeads Human T-Activator CD3/CD28 (Thermo Scientific). Afterwards, only the supernatant (100 µL/well) of activated T cells was added to knocked down tumor cells and incubated overnight at 37°C, 5% CO_2. Luciferase-based cytotoxicity assay was performed. Alternatively, MILs were stimulated with tumor cells at an E:T ratio of 10:1. After 20 h co-culture, plates were centrifuged at 450 g for 5 min and 100 µL/well of the supernatant was collected for cytokines detection (ELISA).

Functional neutralization

For the functional neutralization experiment, anti-FasL (Biolegend) or isotype control (Biolegend) were pre-incubated with MILs for 1 h at 37°C, 5% CO_2. As negative control, antibodies were cultivated in the absence of T cells. Afterwards, antibody-containing supernatants were used to stimulate KMM-1-luc cells, which were reverse transfected with the indicated siRNAs. The final concentration of the neutralizing antibodies was 100 ng/mL for anti-FasL and isotype control. As positive control recombinant FasL protein (100 ng/ml, Biolegend)

was added to the tumor cells instead of T cells. 20 h after co-culture, luciferase intensity was measured.

Blocking assays

For the experiments using the anti-Calmodulin (W7) (Tocris) inhibitor, 1 x 10^4 KMM-1-luc (scr or CAMK1D-transfected) cells/well were seeded in white 96 well plates (Perkin Elmer) in 100 µL of RPMI 10 % FCS. The small molecule inhibitor was added at the indicated concentrations for 1 h at 37°C, before 100 ng/mL rHuFasL or medium control was added. DMSO treatment served as negative control. After 20 h stimulation, luciferase-based cytotoxicity assay was performed. For CAMK1D inhibition, 1 x 10^4 KMM-1-luc or 1 x 10^4 Mel270 cells/well were incubated overnight in a 96 well plate. QPP-A inhibitor (Merck Millipore; CAS 404828-08-6) was added at the indicated concentrations 1h before rHuFasL stimulation (100 ng/ml) or medium control. DMSO treatment served as negative control. After 20h stimulation, luciferase-based cytotoxicity assay was performed.

Luminex assays

Tumor cells were stimulated with rHuFasL (100 ng/mL) for 15 min, 30 min, 1 h, 2 h, 4 h and 8 h. Unstimulated cells served as control. For the detection of intracellular phosphorylated analytes, a general pathway (MILLIPLEX MAP Multi-Pathway Magnetic Bead 9-Plex kit, Millipore) was used. For the detection of proteins involved in the activation of apoptosis the MILLIPLEX MAP Early Phase Apoptosis 7-plex-kit (Millipore) together with active caspase-3 Magnetic Bead MAPmate (Millipore) was used. Beads specific for GAPDH served as normalization control. 20 µg of protein lysates were used for the detection of ERK/MAP kinase

1/2 (Thr185/Tyr187), Akt (Ser473), STAT3 (Ser727), JNK (Thr183/Tyr185), p70 S6 kinase (Thr412), NF-kB (Ser536), STAT5A/B (Tyr694/699), CREB (Ser133), and p38 (Thr180/Tyr182) phosphorylated Akt (Ser473), JNK (Thr183/Tyr185), Bad (Ser112), Bcl-2 (Ser70), p53 (Ser46), cleaved caspase-8 (Asp384), cleaved caspase-9 (Asp315) and active caspase-3 (Asp175). The assay was performed according to the manufacturer´s instructions and samples were measured using the MAGPIX Luminex instrument (Merck Millipore).

High-throughput RNAi screening

Primary RNAi screening

The primary RNAi screening was conducted using a sub-library of the genome-wide siRNA library siGENOME (Dhamacon, GE healthcare), which comprised 2887 genes (1288 genes for GPCR/kinase and 1599 genes for custom library). The library was prepared in Prof. Boutros´s group (DKFZ, Heidelberg) as described in (44). Each well contained a pool of four non-overlapping siRNAs (SMARTpool) targeting the same gene. This arrayed screening approach was performed in duplicates and was adopted from Khandelwal et al (45). Samples siRNA sequences were distributed in the 384-well plates and positive and negative siRNA controls were added in empty wells. Final concentration of all siRNA sequences was 25 nM. Reverse transfection was performed. The read-out was performed using Mithras LB 940 microplate Reader with a counting time of 100 msec. The screening procedure was run in parallel with a CellTiter-Glo luminescent cell viability (CTG) assay on luciferase-negative KMM-1 cells without the addition of MILs in order to exclude genes affecting cell viability. Briefly, for the read-out, supernatant was removed in each well containing siRNA-transfected tumor cells and 20 µL of the CTG reagent (pre-diluted 1:4 in RPMI) were added. After 15 min incubation in the

dark, plates were measured using the Mithras reader as described above. For the screening analysis the raw RLUs from the primary screening, were processed using the cellHTS2 package in R/Bioconductor (46). Values from both conditions were quantile normalized against each other using the aroma.light package in R. Differential scores (cytotoxicity vs. viability) were calculated using the LOESS local regression method. To identify candidate hits, the following thresholds were applied on the z-scores of the samples: for the viability setting, genes showing a $z > + 2,0$ or $z < - 2,0$ were excluded. For the cytotoxicity setting, CCR9 was used as threshold score. Additionally, genes having a z-score $> + 0,5$ or $< - 0,5$ in the CTG-based viability screening were filtered out from the candidate list.

Secondary screening

For the secondary screening, a customized library containing 128 genes from the primary screening was distributed in several 96-well plates along with positive and negative siRNA controls. Reverse transfection was performed. For the cytotoxicity setting MILs (10:1 ratio) were added to knockdown tumor cells (1×10^4 cells/well). Instead, CLM medium was added to the viability plates. After 20 h, luciferase-based read-out was performed. Cytotoxicity/viability ratios were calculated according to the formula:

Cytotoxicity/viability ratio = (Norm. RLU cytotoxicity setting / Norm. RLU viability setting)

by using mock as negative control. The hit-list was generated by including only hits with improved T cell mediated cytotoxicity over mock transfection, (Cytotoxicity/viability ratio < 1). Pearson´s correlation was calculated with Microsoft Excel.

***In vivo* experiment**

Experiments were performed in two cohorts of mice: C57BL6 (n=12) and NOD/SCID gamma chain (NSG) mice (n=12) were subcutaneously injected with 1 x 10^5 MC38 Camk1d KO (g3 clone 11) or 1 x 10^5 MC38 NTS (clone 12) cells each into the right and left flank of one mouse, respectively. Tumor growth was measured twice a week and the volume was determined using the following formula: Tumor volume (mm^3) = ($Width^2$ x Length) x (π / 6). Mice were sacrificed when tumors exceeded 1.5cm in diameter.

Statistics

For statistical analysis, GraphPad Prism software v6.0 (GraphPad Software, La Jolla, CA, USA was used. If not differently stated, statistical differences between the control and the test groups were determined by using two-tailed unpaired Student's t-test. In all statistical tests, a p-value $\leq$ 0.05 was considered significant with * = $p \leq 0.05$, ** = $p \leq 0.01$, *** = $p \leq 0.001$ and **** = $p \leq$ 0.0001.

Study approval

Patients and healthy donors have been included in the study approved by the ethics committee (#229/2003 and S-152/2010) after written informed consent. Animal experiments were approved by the National Ethical Committee for Animal Research (# 5-1/2018/DEMÁB).

Results

MM cells express multiple genes that confer intrinsic resistance towards T cell attack

In order to identify novel genes involved in immune escape mechanisms of PD-L1 unresponsive cancer cells, a high-throughput screening approach recently developed in our laboratory (45) was adapted. The HLA-A2 positive human multiple myeloma cell line KMM-1 was used as a tumor model in this study because KMM-1 cells express high levels of PD-L1 and also lower levels of another recently characterized immune-checkpoint molecule, CCR9 (45). As a reporter system for tumor cell survival we stably transfected KMM-1 cells with e-GFP-firefly luciferase, allowing to apply luminescence imaging as a reliable parameter for immune mediated tumor cell destruction in a HTP format (Figure 1A).

As a source of tumor-reactive T cells we used marrow-infiltrating, PD-1 positive T cells (MILs) from an HLA-A2-matched patient (Figure 1A and supplemental Figure 1A). These MILs were not terminally exhausted as they showed strong IFN-gamma secretion after polyclonal stimulation, which even exceeded that of a well-established tumor antigen specific $CD8^+$ cytotoxic T cell clone, SK-1 (Survivin TC) (45). Moreover, they recognized and reacted by substantial IFN-gamma secretion also against KMM-1 tumor cells, despite high levels of PD-L1 expression on KMM-1 cells (Figure 1B). However, they exerted only limited capacity to kill KMM-1 cells (20 % killing at 10:1 E:T ratio with 5000 KMM-1-luc cells; supplemental Figure 1B) suggesting the presence of resistance mechanisms against T cell attack in KMM-1 cells. Silencing of firefly-luciferase (siFLuc) was used as positive control for siRNA transfection efficacy, while silencing of genes essential for tumor cell survival, such as ubiquitin C (UBC) or transfection with a mixture of siRNAs inducing cell death (siCD) resulted in strong reduction of luciferase expression, indicating appropriate gene silencing and sensitivity of the luciferase-

508 based readout. (Figure 1C). This was also maintained upon co-culture of siRNA treated KMM-1
509 cells with MILs for 20h.
510 We next studied the effect of silencing the immune-checkpoint genes PD-L1 and CCR9 on
511 KMM-1 cells (Figure 1D). Interestingly, the knockdown of PD-L1 did not result in increased
512 killing of KMM-1 cells by MILs, despite high expression of PD-L1 on the tumors and of PD-1
513 on the MILs. In contrast, the knockdown of CCR9 significantly improved tumor cell rejection
514 (Figure 1E), suggesting that PD-L1 did not play a decisive role in resistance of KMM-1 cells
515 against the cytotoxic T cell attack. We therefore used CCR9 as positive control within the siRNA
516 screen.
517 To this end, KMM-1 cells were transfected in a multi-well format with a siRNA library
518 consisting of a pool of four individual non-overlapping siRNAs per target per well, targeting a
519 total of 2887 genes (supplemental Table 1) covering a broad spectrum of all gene families. The
520 workflow of the screening approach comprised a viability control setup, in which we assessed
521 the intrinsic viability effect of each gene knockdown *per se*, and a cytotoxicity setting, in which
522 siRNA transfected tumor cells were co-cultured with MILs (supplemental Figure 2).
523 Negative (scramble siRNA sequences, scr1 and scr2) and positive controls (siRNAs-targeting
524 luciferase and essential viability genes such as UBC) were included as a reference to calculate
525 the effect of gene knockdown on cell viability. Overall, the distribution of values across test
526 replicates and setups was highly concordant showing no viability or cytotoxicity effect of scr
527 siRNAs but robust signal reduction after FLuc and UBC knockdown (Figure 2A). Calculated z
528 scores for the impact on cell viability and T cell cytotoxicity (Figure 2B) and for the relative
529 impact on T cell mediated tumor cell lysis (Loess score; Figure 2C) of each gene revealed 128
530 genes whose silencing improved tumor cell lysis by T cells to a higher degree than the positive

control CCR9. Among them we found several genes with described immune regulatory function in multiple myeloma such as CD5 (47) , FES (48) and PAK3 (49). In line with the literature and with the previous setup of positive controls, PD-L1 did not show any effect on T cell mediated killing of multiple myeloma cells. The identification of these validated immune-checkpoints in combination with good immune-checkpoint control performance supported the robustness and sensitivity of the screen.

For further validation, we subjected the 128 candidate hits to a secondary screening procedure using the same setup as for the HTP screen. Silencing of 90 candidates identified in the HTP-screen again increased T cell mediated killing of tumor cells and exerted only little effects on intrinsic tumor cell viability, thus confirming their immune regulatory role in KMM-1 cells (Figure 2D). The strongest immune modulatory effect (high impact on T cell killing and no viability impact) was elicited by the serine/threonine calcium/calmodulin-dependent protein kinase 1D (CAMK1D) (Figure 2B-D).

In order to determine whether the observed tumor cell killing was mediated by cytokines or other soluble proteins released by activated MILs into the supernatant, an additional setting was included in the secondary screening. Hence, MILs were polyclonally stimulated with anti-CD3/anti-CD28 magnetic beads for 20h and only their cell culture supernatant was added to the tumor cells. In this control setup silencing of only few genes showed an impact on tumor cell lysis indicating for these genes a role in resistance towards T cell secreted cytotoxic cytokines (Figure 2E). Although we cannot exclude the possibility that we may have missed relevant cytokines secreted by T cells upon their contact with tumor cells, most of the identified candidate genes, including CAMK1D, regulated tumor cell killing only upon direct interaction with T cells.

553 Taken together, these results provide a first indication that multiple myeloma cells express
554 multiple immune regulatory genes, among them CAMK1D, that confer immune resistance after
555 T cell engagement.
556
557 **CAMK1D protects PD-L1$^+$ tumor cells against death receptor signaling by cytotoxic T cells**
558 Based on the strong immune resistance phenotype associated with CAMK1D expression in the
559 screens, we further on focused on validation and characterization of the immune regulatory role
560 of this kinase. So far, an immune-related function of CAMK1D in cancer evasion has not been
561 studied. We first de-convoluted the pool of CAMK1D targeting siRNAs used in the HTP-screen
562 to exclude potential dominant off-target effects of single siRNAs within the pool. Three out of
563 four CAMK1D targeting siRNAs (s1, s2 and s3) and the pool of all siRNAs increased T cell
564 mediated cytotoxicity, while no viability impact of the individual or pooled siRNAs *per se* was
565 detected (Figure 3A) and all of them significantly reduced CAMK1D expression at mRNA and
566 protein level (Figure 3B, C). In a luciferase-independent assay, employing live cell-imaging of
567 tumor cell apoptosis using a fluorescence apoptosis dye (YOYO-1) we could confirm a strong
568 increase of MIL-induced apoptosis in CAMK1D-deficient KMM-1 cells (Figure 3D). This could
569 be inhibited by MHC-I blocking antibodies, indicating that tumor cell apoptosis was induced by
570 MHC-I-restricted CD8$^+$ MILs in a T cell receptor-dependent manner (Figure 3E). To corroborate
571 this further, we pulsed KMM-1 cells with an HLA-A2-restricted peptide of influenza-matrix
572 protein and co-cultured them with PD-1 positive, influenza (flu)-peptide-specific CD8$^+$ cytotoxic
573 T cells (flu TC) (supplemental Figure 3A). Again, CAMK1D silencing but not PD-L1 silencing
574 (data not shown) resulted in a significant increase of T cell-mediated tumor cell lysis (Figure 3F),
575 demonstrating that CAMK1D mediates resistance of KMM-1 cells towards an attack by antigen

specific cytotoxic T cells and that this effect occurs independent of the T cell source. Of note, CAMK1D mediated immune protection not only in KMM-1 cells but to a comparable degree also in an additional PD-L1^{+}, HLA-A2^{+} multiple myeloma cell line, U266 (Figure 3G-I and supplemental Figure 3B). We therefore studied CAMK1D expression in a large cohort of CD138-purfied malignant plasma cells from multiple myeloma patients with monoclonal gammopathy of unknown significance (MGUS), human myeloma cell lines (HMCL), memory B cells (MBC), plasmablasts (PPC) and normal bone marrow plasma cells (BMPC). CAMK1D expression was highest in MBC but it was also expressed in all MM, MGUS, PPC, and in 30/32 HMCL samples and these showed higher expression than normal bone marrow plasma cells (BMPCs) (Figure 3J). Thus, these data indicate that CAMK1D is consistently expressed in human multiple myelomas and confers resistance against cytotoxic T cell attack. Classical immune-checkpoint molecules expressed by tumor cells regulate the activity of cytotoxic T cells mostly through engagement of inhibitory receptors on T cells. Since CAMK1D is an intracellular kinase, we wondered whether it may indirectly regulate T cell activity. We therefore studied parameters of T cell effector function upon contact with CAMK1D proficient or deficient KMM-1 cells, including the secretion of the T cell effector cytokines INF-γ, Granzyme B, IL-2 or TNF-α. Although we consistently detected increased T cell-mediated tumor cell killing after CAMK1D knockdown in KMM-1 cells, functional analysis of T cells did not reveal any increased T cell function after interaction with CAMK1D-deficient compared to wt tumor cells (supplemental Figure 3C). Therefore, we concluded that CAMK1D expression in tumor cells does not affect type 1 effector T cell function and hypothesized that it may instead regulate the sensitivity of tumor cells towards cytotoxic T cell attack. Thus, we exposed KMM-1 cells to the cytotoxic agents FasL (rHuFasL), TRAIL (rHuTRAIL) or TNF (rHuTNF) commonly used by T

599 cells to kill their target cells. The respective cell death-mediating receptors for FasL and TRAIL,
600 Fas, DR4 and DR5 were strongly expressed on KMM-1 cells while the TNF receptors TNFR1
601 and TNFR2 were not expressed (Figure 4A). While CAMK1D-proficient KMM-1 cells were
602 resistant against all tested cytotoxic agents, CAMK1D-deficient tumor cells were dramatically
603 reduced after exposure to FasL and, to a much lesser degree, after exposure to recombinant
604 TRAIL (Figure 4B). In line, we detected FasL on 28.2% and 16.1% of $CD4^+$ and $CD8^+$ MILs,
605 respectively (Figure 4C) and on 12.7% of flu TC (supplemental Figure 3D). TRAIL expression
606 was detected only on 12.5% and 5.3% of $CD4^+$ and $CD8^+$ MILs, while membrane bound TNF
607 was hardly detectable (Figure 4C). Neutralization of FasL by monoclonal antibodies completely
608 abrogated the CAMK1D-induced protection against cytotoxic activity of MILs (Figure 4D).
609 Thus, CAMK1D mediates intrinsic tumor resistance against activated T cells through interfering
610 with Fas-mediated death signaling. In line with this, U266 myeloma cells strongly express Fas
611 (Figure 4E) and similar to KMM-1 cells they are protected by CAMK1D expression against Fas-
612 mediated cell death (Figure 4F). Since Fas-FasL interactions represent a major cytotoxic
613 principle in tumor immunology, we wondered whether CAMK1D might protect not only
614 multiple myeloma but also solid tumor cells against immune rejection. We therefore analyzed
615 Fas expression on several human cancer cell lines. Fas expression was low in the pancreatic
616 cancer cell line PANC-1 and in the breast cancer cell line MCF-7. However, we found strong Fas
617 and CAMK1D expression in Mel270, which is a PD-$L1^+$ human uveal melanoma (UVM) cell
618 line (Figure 4G, H and supplemental Figure 4). UVM is a highly treatment-refractory and anti-
619 PD-1-resistant subtype of malignant melanoma (50). In line with the observation in the myeloma
620 cell lines, silencing of CAMK1D significantly increased the cytolytic response of Mel270
621 towards FasL exposure (Figure 4I), indicating that uveal melanomas can exploit CAMK1D for

622 resistance against T cell attack. In contrast, although expressed, CAMK1D silencing in the Fas
623 negative tumor cell lines PANC-1 and MCF-7 did not sensitize these cells towards T cell killing
624 (data not shown). These data indicate a strong rationale for CAMK1D inhibition only in the
625 context of Fas-positive tumors to achieve significant anti-tumor immune response. The clinical
626 outcome of a cohort of uveal melanoma patients together with genome-wide RNA expression
627 data from their tumor tissue is available at the TCGA database and allows an analysis of the
628 prognostic impact of CAMK1D in this highly immunotherapy-refractory patient population. We
629 hypothesized that CAMK1D expression in UVM might protect those tumors with strong Fas
630 receptor expression against immune rejection. We therefore stratified patients in this cohort
631 according to expression levels of CAMK1D and Fas (above/below median). Kaplan-Meier
632 analyses show that overexpression of CAMK1D in Fas receptor^{high} tumors but not in Fas
633 receptor^{low} tumors correlate with poor patient prognosis (Figure 4J). This suggests that
634 CAMK1D exerts a tumor protective effect only in the context of Fas receptor activation during
635 an immune response. T cell activity in tumors is characterized by IFN-gamma secretion and thus
636 correlates with PD-L1 upregulation. We found that over-expression of CAMK1D and PD-L1
637 were tightly co-regulated in UVM melanomas (Figure 4K). Thus, under conditions of immune
638 activation and PD-L1 expression CAMK1D represents another level of immune resistance in
639 tumor cells. Furthermore, our study with PD-L1 expressing yet refractory tumor models shows
640 that CAMK1D supersedes the PD-L1 axis in mediating immune-suppression. Using the TCGA
641 database we studied CAMK1D and PD-L1 co-regulation in other tumor entities that are largely
642 unresponsive to anti-PD-1 treatment, specifically in ovarian, pancreatic, colorectal, stomach and
643 esophageal cancer and in glioblastoma. Among them, CAMK1D and PD-L1 were co-expressed
644 in ovarian, pancreatic, stomach and esophageal cancer. As observed in UVM, we detected

significant correlations of CAMK1D and Fas receptor expression with poor outcome in these cancers (supplemental Figure 5A-F) with the exception of pancreatic cancer. However, pancreatic cancer is characterized by defective Fas receptor signaling (51, 52) and thus CAMK1D-mediated immune protection may not be activated in this tumor entity. Taken together, our data indicate that in several PD-1-therapy refractory tumors, CAMK1D is co-regulated with PD-L1 and controls tumor rejection after Fas receptor activation.

CAMK1D regulates the activity of effector caspases -3, -6 and -7 after Fas receptor activation

FasL binding to Fas receptor results in complex signaling events. This induces on the one hand the caspase cascade that finally activates endonucleases to initiate apoptosis by DNA fragmentation and on the other hand stimulates Ca^{2+} influx into the cytoplasm, which ultimately triggers CAMK1D activation. We therefore speculated that CAMK1D might interfere with the cellular apoptotic cascade to mediate its tumor protective effect. To clarify this assumption, we assessed the impact of CAMK1D expression on tumor cell killing in the absence of effector caspases. Indeed, silencing of each of the individual downstream effector caspase (caspase -3, -6 and -7) completely abrogated the increased lysis of CAMK1D-deficient tumor cells after FasL exposure (Figure 5A, B). Thus, CAMK1D selectively regulates cellular sensitivity towards apoptotic cell death. Besides, these results demonstrate the necessity of simultaneous activity of all three effector caspases for efficient induction of apoptotic cell death after Fas activation.

CAMK1D activation depends on binding to calmodulin (CaM) which upon Ca^{2+} influx induces a conformational change allowing the CAMK-kinase (CAMKK) to phosphorylate and fully activate CAMK1D (53, 54). We speculated that FasL-expressing MILs might trigger Ca^{2+} release in KMM-1 cells sufficient for CAMK1D activation. We therefore compared intracellular

669 Ca^{2+} in KMM-1 cells on single cell level after exposure to MILs or rHuFasL and found that both
670 procedures induced a similar, robust increase of intracellular Ca^{2+} shortly after treatment (Figure
671 5C, D).
672 Activation of CAMK1D requires binding to Ca^{2+}/calmodulin complexes which can be inhibited
673 by W-7 hydrochloride (55). Treatment with 5 μM W-7 hydrochloride is not toxic to KMM-1
674 cells (Figure 5E) and sharply recapitulated the effect of CAMK1D silencing on FasL induced
675 tumor cell apoptosis, suggesting CAMK1D to be the decisive target of calmodulin for mediating
676 FasL resistance (Figure 5F). Since both CAMK1D silencing (50%-75% knockdown efficiency)
677 and W-7 hydrochloride treatment only incompletely blocked CAMK1D, we also explored
678 whether their combination further reduced cell viability after FasL exposure. Indeed, this
679 combinatorial treatment resulted in a 3-fold further increase of FasL-mediated tumor cell killing
680 (Figure 5F). To corroborate these findings, we applied CAMK1D –inhibitor (QPP-A) to the
681 multiple myeloma as well as the uveal melanoma cell line. The additional treatment with
682 recombinant FasL induced a significant loss of tumor cell viability, confirming that CAMK1D
683 plays a substantial role in conferring resistance towards tumor cell apoptosis (Figure 5G).
684 Taken together, these results demonstrate that CAMK1D activation in cancer cells is (i) triggered
685 by cytotoxic T cells via FasL-induced Ca^{2+} release and (ii) is required to control Fas-induced
686 tumor cell apoptosis. To further confirm the role of CAMK1D in mediating cancer resistance
687 against immune attack *in vivo*, we knocked out Camk1d in the murine colorectal cell line MC38
688 using the CRISPR/Cas9 technique (Supplemental Figure 6A). *In vitro* analysis of MC38
689 Camk1d-deficient tumor cells revealed their increased sensitivity towards FasL as well as
690 TRAIL mediated apoptosis (Supplemental Figure 6B). Thus, we injected MC38 Camk1d KO as
691 well as MC38 NTS (non-targeting sequence) cells into the left and right flank of the same mouse

of both immunodeficient NSG and immunocompetent C57BL6 mice. MC38 Camk1d KO and MC38 NTS tumors developed rapidly in a similar manner in NSG mice, while a significant difference was observed in the immunocompetent C57BL6 mice, where Camk1d-wt tumors showed rapid outgrowth similar to that the NSG mice, while the growth of Camk1d-deficient tumors was significantly retarded (Figure 5H). These data demonstrate that the immune system in immunocompetent mice was not able to retard the outgrowth of MC38 cells due to the expression of Camk1d.

To elucidate mechanistic aspects of CAMK1D involvement in the Fas-signaling cascade, we studied activation of caspase-8 and -9, the prototypic initiator caspases of the extrinsic and intrinsic apoptotic pathway, respectively (56). FasL-induced activation of caspase-8 and -9 was comparably effective in CAMK1D proficient and –deficient KMM-1 cells (Figure 6A, B). Thus, CAMK1D controls initiation of the apoptotic cascade downstream of death inducing signaling complex (DISC) assembly or activation of initiator caspases. Consequently, we hypothesized that CAMK1D regulates the activity of effector caspases -3, -6 or -7. To this end, we first studied the activation of the central executioner caspase-3 through various techniques, including Luminex analysis, flow cytometry and western blot. Indeed, we observed a strong increase in caspase-3 activation in CAMK1D-deficient KMM-1 cells after FasL treatment (Figure 6C-E). In addition, we also detected increased cleavage of the effector caspases -6 and -7 in CAMK1D-deficient tumor cells (Figure 6F and supplemental Figure 7A). Moreover, the phosphorylation and thus activation level of the transcription factor cAMP response element-binding protein (CREB), was increased in CAMK1D-proficient cells, which was responsible for the transcription of the anti-apoptotic molecule Bcl-2. We also observed that at early time-points (15min, 30min and 1h) of rHuFasL stimulation the phosphorylation levels of the Extracellular Signal-regulated

715 Kinases (ERK1/2), were enhanced in wild-type cells, while the knockdown of CAMK1D re-
716 established basal levels (Supplemental Figure 7B). The altered activation of the presented
717 proteins implies that CAMK1D not only controls activation and activity of effector caspases but
718 also induces the expression of anti-apoptotic and mitogenic proteins of KMM-1 cells leading to
719 tumor cell resistance towards FasL-positive T cells. CAMK1D has thus far not been established
720 as a regulator of effector caspase activity. Notably, in silico analysis (using the webtools
721 KinaseNet and UniProt (http://www.kinasenet.ca/showProtein;
722 https://www.uniprot.org/uniprot/P42574) predicted a binding motif for CAMK1D on caspase-3
723 and also on caspase-6 (supplemental Figure 7D). For caspase-7, however, no binding motifs
724 were predicted. To confirm these results, we performed co-immunoprecipitation (co-IP)
725 experiments. Notably, CAMK1D co-immunoprecipitated with caspase-3, caspase-6, and
726 caspase-7 and the levels of CAMK1D interaction with all three effector caspases increased upon
727 rHuFasL treatment (Figure 6G, H and supplemental Figure 7C). A direct CAMK1D/effector
728 caspase interaction could on the one hand result in stoichiometric inhibition of caspase cleavage
729 by initiator caspases. Alternatively, the effector caspases may also serve as targets of CAMK1D
730 kinase activity. Phosphorylation of inhibitory serine residues 150 (caspase-3) or 257 (caspase-6)
731 impedes their activation, proteolytic activity and ultimately hampers apoptosis induction (57).
732 Notably, the inhibitory Ser150 phosphorylation site of caspase-3 (58) and the corresponding
733 Ser257 of caspase-6 (59) are located in the kinase-function critical distance of up to 4 amino
734 acids apart from the predicted binding site for CAMK1D (supplemental Figure 7D). We
735 therefore wondered whether CAMK1D is able to phosphorylate Ser150 and Ser257 of caspases -
736 3 and -6. Indeed, CAMK1D deficient KMM-1 cells showed a strongly reduced phosphorylation
737 level of inhibitory serine residues of both caspase-3 and -6 already at steady–state conditions

738 (Figure 6I-L). In KMM-1 wt cells, phosphorylation levels transiently decreased 15min - 30min
739 after FasL treatment (which has been attributed to transient stimulation of phosphatases (60)),
740 but recovered to pre-stimulation levels within 1h (caspase-3) to 4h (caspase-6). In contrast,
741 caspase-3 and -6 phosphorylation was persistently low in CAMK1D-deficient KMM-1 cells
742 throughout the entire observation period, resulting in overall much lower caspase inactivation
743 compared to CAMK1D wt cells. This demonstrates that CAMK1D is required for steady-state
744 inactivation of effector caspases through phosphorylation and for the rapid restoration of
745 caspase-3 and -6 phosphorylation after FasL stimulation.
746 Taken together, these results demonstrate that in tumors, CAMK1D upon its activation through
747 FasL regulates activation and activity of all effector caspases after cytotoxic T cell encounter.
748 These results further suggest that this is at least partially achieved by the inhibitory
749 phosphorylation of the effector caspases.
750

Discussion

We here used a multiple myeloma cell line to conduct a systematic search for genes controlling immune rejection in PD-L1 refractory human tumors. Such tumors, including amongst others, multiple myeloma, are defined by the lack of clinical efficacy of PD-L1 or PD-1 -inhibition and are therefore largely unresponsive to cancer immunotherapy, so far. PD-L1 unresponsiveness was also given for the experimental setup used in this screen since PD-L1 silencing did not improve immune rejection *in vitro* despite expression of PD-L1 on the tumor cells and of PD-1 by the patient-derived cytotoxic T cells. The screen revealed 90 genes which controlled tumor cell killing by T cells. Among them, the serine/threonine kinase CAMK1D exerted the strongest protective effect against myeloma-reactive cytotoxic effector T cells. CAMK1D belongs to the multifunctional CaM-kinases whose activation is dependent on the initial binding of calcium and calmodulin. To date, little is known about the role of CAMK1D in cancer. However, CAMK1D expression is elevated in invasive carcinomas compared to carcinoma in situ and by overexpressing CAMK1D in non-tumorigenic breast epithelial cells an increased proliferation, and epithelial-mesenchymal transition was observed (61). Here, we report a different role of CAMK1D in controlling the resistance of PD-L1^{+} tumor cells against apoptosis triggered by cytotoxic T cells.

CAMK1D was co-expressed with PD-L1 in several largely anti-PD-1 treatment refractory tumors such as ovarian, gastric and esophageal cancer and uveal melanoma and patients with these tumors experienced better survival if CAMK1D expression was absent or low. These observations support the conclusion that CAMK1D expression represents a relevant mechanism of immune resistance in human cancer. However, future studies should address the relevance of this pathway in primary human tumor cells such as multiple myeloma freshly isolated from

774 patients. Indeed, CAMK1D-deficient tumor cells showed an increased activation and decreased
775 functional inhibition of effector caspases through inhibitory phosphorylation. We could not
776 perform a phosphorylation-specific analysis for caspase-7, because phospho-specific antibodies
777 were not available for this caspase. Nevertheless, CAMK1D co-precipitates with all three
778 effector caspases suggesting that it can directly bind to effector caspases and thereby on the one
779 hand inhibits their activation, acting as a stoichiometric inhibitor of caspase cleavage and on the
780 other hand inhibits effector caspase function directly by phosphorylation. As the cellular levels
781 of CAMK1D (as 'measured' by Western Blot) do not change upon exposure to FasL for 4h, it
782 appears unlikely that the observed FasL-induced increase in caspase-associated CAMK1D is
783 attributable to e.g. enhanced de novo synthesis of CAMK1D and subsequent increase in non-
784 specific binding.
785 Since CAMK1D aggregation with effector caspases was increased after FasL stimulation, this
786 mechanism of apoptosis resistance appears to be triggered by the cytotoxic T cells themselves.
787 This occurs most likely through Fas-mediated Ca^{2+} influx and subsequent calmodulin activation
788 because calmodulin activity was required for the protective function of CAMK1D.
789 Cytotoxic T cells eliminate tumor cells not only through the extrinsic apoptosis pathway which is
790 initiated by death receptor signaling through FasL, TRAIL or TNF and mediated by activation of
791 pro-caspase-8 (62-64), but in addition through triggering the intrinsic or mitochondrial pathway
792 through the release of cytotoxic granules which induces mitochondrial damage, apoptosome
793 formation and subsequent activation of pro-caspase-9 (65). Both initiator caspases activate the
794 common executioner caspases -3, -6 and -7, which in turn cleave key intracellular substrates
795 within the cells including endonucleases, thus irreversibly triggering the apoptotic cell death (66,
796 67).

We observed that the initiator caspases -8 and -9 were not differentially affected in CAMK1D proficient and –deficient tumor cells. In line, as shown by IR Powley et al. (68) Caspase-8 is inactivated upon phosphorylation of a tyrosine residue (Y380), which leads to increased resistance to CD95-induced apoptosis. However, CAMK1D is a serine/threonine protein kinase and in silico analysis revealed no binding site between CAMK1D and Caspase-8.

Co-expression of death receptor ligands and cytotoxic granules thus enable CTL to simultaneously trigger both apoptosis pathways and by this capacity, they differ from other common mechanisms of cell apoptosis, which generally trigger either one or the other apoptotic pathway. Therefore, efficient resistance mechanisms against T cell-induced apoptosis need to target the common end route of both pathways. Consequently, inhibition of effector caspase activity may represent a hallmark of tumor immune resistance.

Inhibition of effector caspases to control CTL-induced cytotoxicity needs to be strictly regulated as its constitutive activation in a cell would result in general resistance against all other physiological apoptosis stimuli and this would not be compatible with self-regulation of multicellular systems. Therefore, it is conceivable that the activation of mechanisms protecting against T cell-induced apoptosis requires CTL-specific stimuli and needs to be restricted to the period of ongoing T cell attack.

In the past, a variety of mechanisms to regulate apoptosis have been identified and these are commonly exploited by tumor cells. The majority of these controls the apoptotic cascade upstream of effector caspases. For example, some tumors regulate the extrinsic apoptosis pathway through impaired expression of death receptors of their downstream signaling components, through reduced expression of pro-caspase-8 or through overexpression of anti-apoptotic molecules such as c-Flip, thereby preventing the activation of pro-caspase-8 at the

DISC (69, 70). Resistance against most anti-cancer agents can be acquired through regulation of the mitochondrial apoptosis pathway by reduced expression of basic components of the apoptosome such as Apaf-1, upregulation of the anti-apoptotic gene *BCL2* or downregulation of the pro-apoptotic *BAX*-gene (71, 72).

In contrast, so far only few molecules are known to directly interfere with the proteolytic activity of effector caspases. The most prominent are the inhibitor of apoptosis protein (IAP) family members X-IAP and survivin, which possess a binding domain for the protease subunit of the effector caspases -3 and -7 together with a ubiquitinylation domain and thus are able to sterically inhibit the activity of these two caspases (though not of caspase-6) and to initiate their degradation (73).

However, it is questionable whether IAPs represent appropriate regulators of CTL-induced apoptosis, since their activity is not particularly tunable by T cell signals. Instead, activity of X-IAP and survivin is largely determined by fairly constant baseline transcriptional expression levels - which can be adapted under conditions of cellular stress such as DNA damage, COX signaling or hypoxia and by exposure to the immune suppressive cytokine TGF-ß (74), or upon triggering of cell cycle progression through EGF or IGF-1 (75), respectively. Moreover, the activity of both molecules is reduced upon intrinsic apoptosis signaling through release of the mitochondrial protein Smac which inhibits the caspase binding domain of the IAPs (76). Thus, regulation of IAP activity appears to follow a rather slow kinetic largely adapted to chronic stimuli.

Therefore, additional levels of apoptosis control are required, which provide an immediate protection against selective stimuli such as an immune attack. For this, kinases may be much more suitable as they are activated within seconds after the signal is received and can

immediately inhibit the terminal level of the apoptotic cascade by inhibition of effector caspases through binding and phosphorylation. Indeed, effector caspase activity can be regulated by phosphorylation (57). However, so far only two kinases, p38 MAPK which selectively binds to effector caspase-3 and ARK5, selectively binding to caspase-6, were reported to phosphorylate their targets at inhibitory serine residues (59). Both kinases are expressed and activated similar to IAPs upon conditions of cellular stress (77, 78) and in addition, ARK5 activity can be triggered by TRAIL and TNF (79). However, to our knowledge, a mechanism triggered by FasL and controlling simultaneously the activity of all three effector caspases has not been reported so far.

To support the clinical applicability of CAMK1D blockade, we took advantage of small molecule compounds. One concern about CAMK1D targeted pharmacologic inhibition may be its ubiquitous expression particularly in T cells and neurons. Thus, inhibition of this protein kinase could on the one hand increase tumor susceptibility towards T cell attack, but on the other hand impair T cell activity. In line with this concern, Bellucci and colleagues demonstrated that the blockade of the tyrosine kinase, JAK2, sensitized multiple myeloma tumor cells towards the attack of NK cells (80). Nevertheless, recent clinical studies showed that JAK1/2 inhibitors impair the functionality of NK cells and T cells in myeloproliferative neoplasms (81-83). Consequently, supplementary studies must be conducted to clarify the exact role of CAMK1D inhibition in T cells and which consequences a targeted therapy would have on neurons. Nonetheless, CAMK1D remains an interesting target for cancer immunotherapy, in particular for those patients who experience relapse or demonstrate unresponsiveness to conventional therapies.

Consistently, our studies conducted in mice already confirmed the role of CAMK1D *in vivo* as a novel immune-checkpoint molecule conferring resistance towards the immune attack.

Altogether, it is conceivable that tumor cells exploit Fas receptor signaling imposed by cytotoxic T cells to activate an apoptosis resistance mechanism targeting the final effector level of both intrinsic and extrinsic apoptotic pathway resulting in an increased resistance against immune cell attack even upon immune-checkpoint inhibition. Besides, in T cell infiltrated tumors this mechanism may also impact on the general treatment resistance of tumor cells, because CAMK1D could reduce the efficacy of most anti-cancer treatments including chemotherapy, irradiation and targeted therapies used in clinical oncology, which all directly or indirectly exploit the intrinsic apoptotic signaling pathways to trigger cancer cell death.

Acknowledgments: We thank Dr. R. Haase (LMU, Munich) for the pEGFP-Luc plasmid, Prof. G. Moldenhauer (DKFZ, Heidelberg) for the generation of the MHC-I and isotype antibodies.

Author contributions: VV, TM, AS, ANM, GK, MD, VMM, CYC and ASz performed experiments and VV and TM conducted bioinformatics analyses. VV, TM, AS and PB designed, conducted and analyzed the HTP screen. VV and PB designed the study and drafted the manuscript. All authors contributed to the manuscript preparation.

Figures

Figure 1

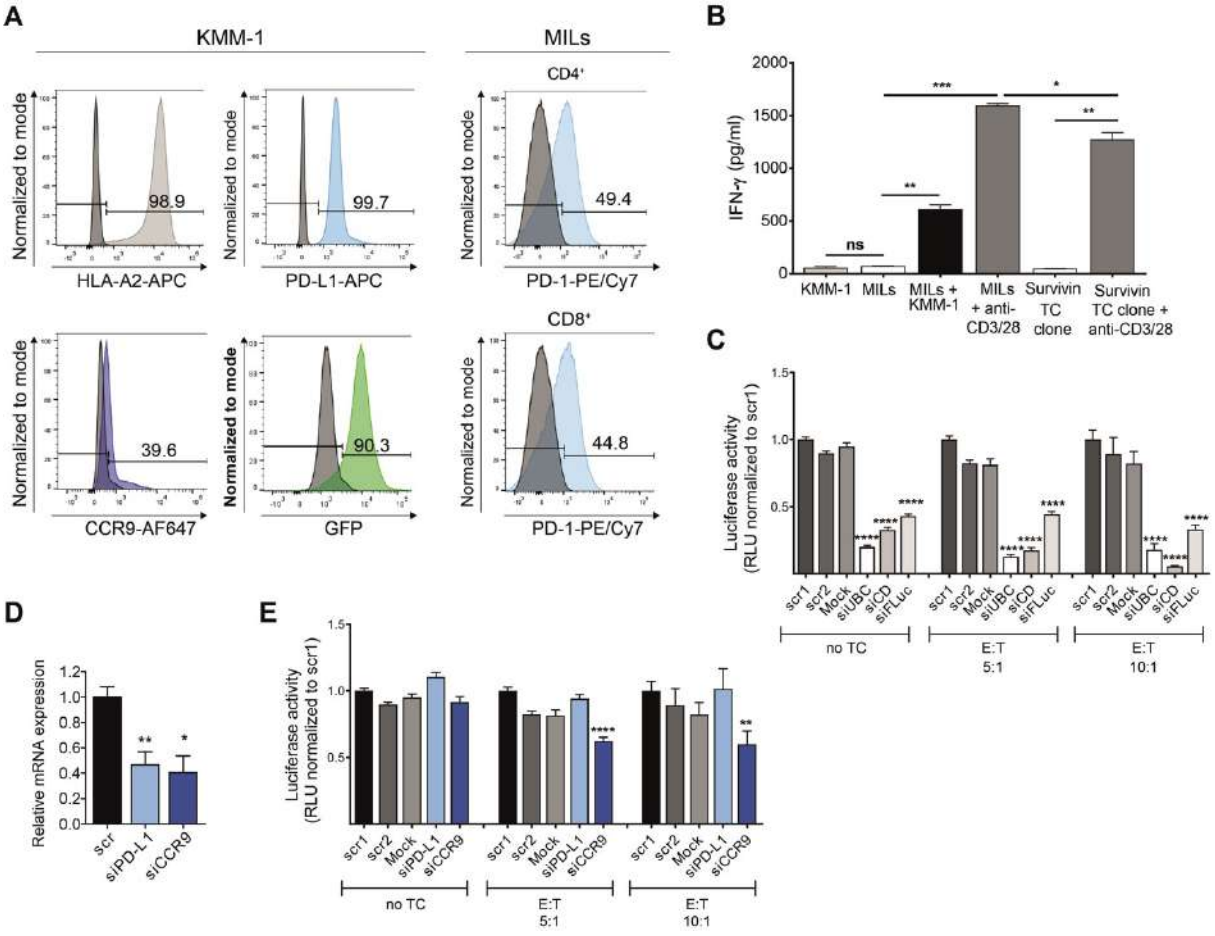

Figure 1. Assessment of positive and negative immune-checkpoint controls for the HTP-screen. **(A)** Left: FACS-analysis of HLA-A2 (light grey histogram), PD-L1 (blue histogram), CCR9 (dark blue histogram) and GFP (green histogram) on KMM-1 cells. Isotype is shown as dark grey histogram. Right: FACS-staining on CD4 and CD8 –positive MILs. Cells were stained with anti-PD-1 (light blue) antibody and subsequently analyzed by FACS. Isotype control is shown as dark grey histogram. **(B)** MILs and KMM-1 cells were co-cultured for 20h. IFN-γ secretion was measured by ELISA. As negative control, MILs and Survivin TC clones were cultured in the absence of tumor cells. Background INF-γ was measured in KMM-1 cells alone. Anti-CD3/anti-CD28 magnetic beads stimulated MILs or Survivin TC clones were used as positive control. **(C)** KMM-1-luc cells were transfected with the specified siRNA sequences. Loss of luciferase activity was compared to negative siRNA sequences. Statistical significance was calculated compared to scr1 siRNA sequence. Knocked down tumor cells were co-cultured with MILs in different E:T ratios. **(D)** Quantitative PCR (qPCR) analysis of CCR9 and PD-L1 mRNA expression in KMM-1 cells after 48h siRNA transfection. Results are presented in terms of fold change after β-actin mRNA normalization. **(E)** KMM-1-luc cells were transfected with the indicated siRNA sequences for 48h. Luciferase-based viability assay was conducted (no TC control) and co-culture with MILs at indicated E:T ratios was performed for cytotoxicity assay. Cell survival was determined by measuring the remaining luciferase activity of tumor cells after 20h co-culture with MILs or culture medium (no TC). **(B, C, D, E)** Graphs show mean +/- SEM of at least two independent experiments. P-values were calculated using unpaired two-tailed student´s t-test. * $p < 0.05$, ** $p < 0.01$, *** $p < 0.001$, **** $p < 0.0001$

Figure 2

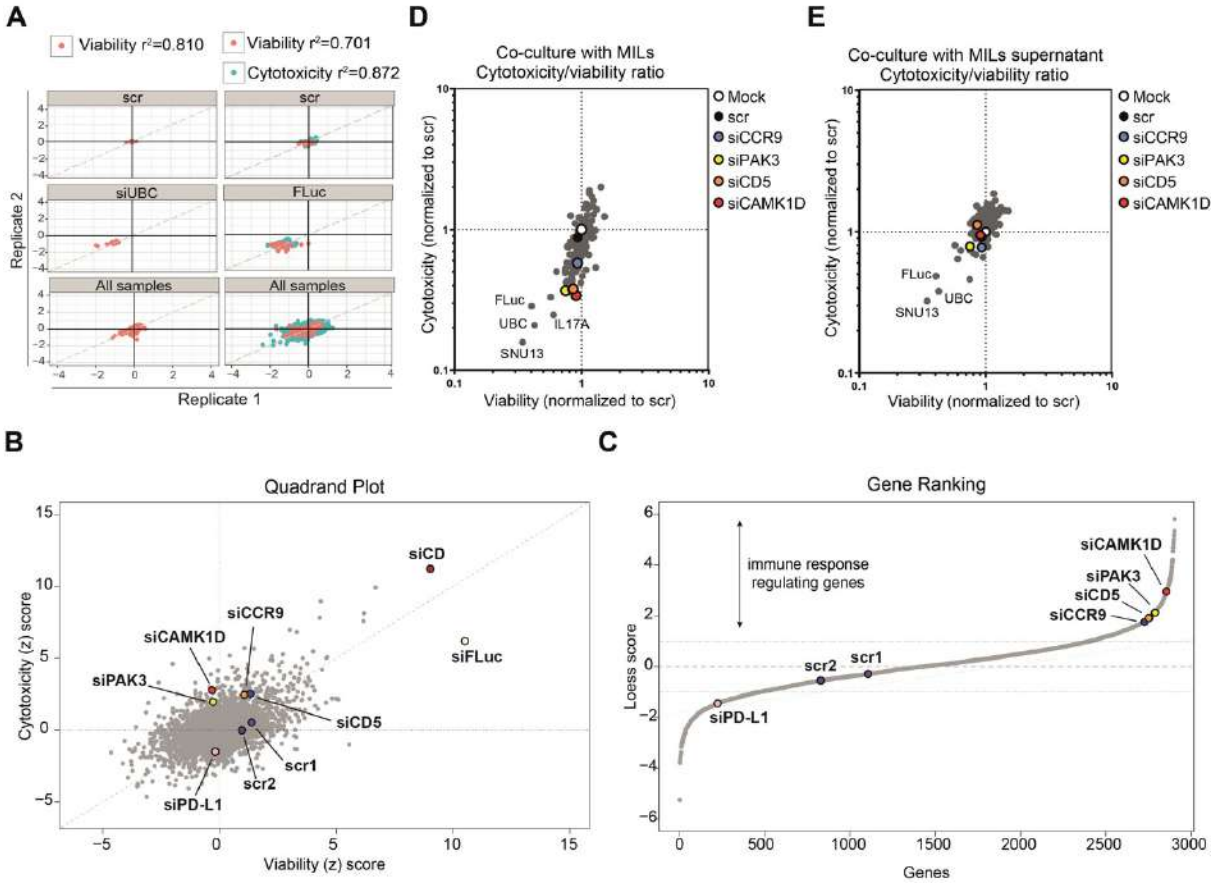

Figure 2. Performance of the HTP screen. (A) Dot plot shows normalized and scored RLUs after transfection of KMM-1 wt or KMM-1-luc cells with several control siRNAs. Technical replicates were plotted against each other. Left: 20 x 384-well plates were subjected to the luciferase-independent CellTiter-Glo (CTG) screening performed on KMM-1 wt cells in which cell viability was determined by measuring intracellular ATP levels. Right: 40 x 384-well plates were subjected to the luciferase-based screening assay performed on KMM-1-luc cells. Blue dots: cytotoxicity setting (tumor cells co-cultured with MILs). Red dots: viability setting (tumor cells without MILs). Pearson correlation (r^2) between the 2 replicate values was calculated for each setting. **(B)** Quadrant plot showing z-scores of gene knockdown in transfected KMM-1-luc cells after co-culture with MILs (cytotoxicity z-score) or with culture medium (viability z-score), using a siRNA library of 2887 genes. **(C)** Gene ranking diagram showing differential score between cytotoxicity and viability z-scores using local regression (LOESS) rank. The upper panel classifies the potential immune response regulating genes with a high loess score in multiple myeloma cells. Genes with differential score higher than CCR9 knockdown were selected as potential negative immune-modulators. **(D, E)** Secondary screening results: Luciferase-based secondary screening was performed using the hits obtained from the primary screening. Knocked down tumor cells were co-cultured with (D) MILs or (E) supernatant of anti-CD3/anti-CD28 magnetic beads activated MILs. RLUs were normalized to Mock siRNA control. Log2 scale of cytotoxicity/viability ratio is depicted. Experiments were performed in duplicates. Mean is shown.

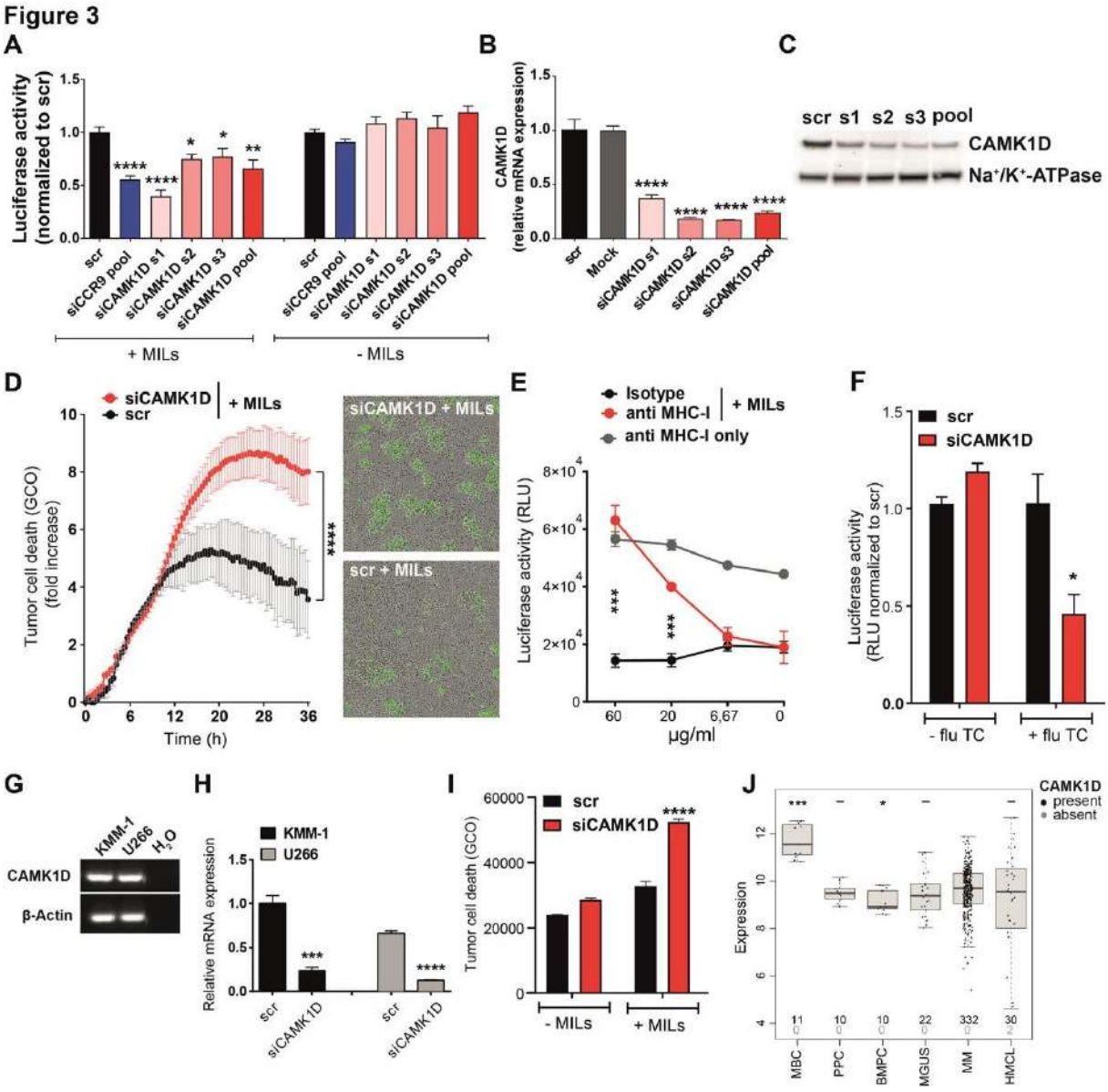

Figure 3. Validation of siCAMK1D effect. (A) KMM-1-luc cells were transfected using single (s1, s2, s3) or pooled non-overlapping siRNAs targeting CAMK1D. Control siRNA (scr) was used as a negative control, whereas pooled siCCR9 served as positive control. Transfected cells were co-cultured with MILs at 10:1 E:T ratio for the cytotoxicity setting. For the viability setting, only culture medium was added instead of T cells. T cell-mediated cytotoxicity was measured using the luciferase-based cytotoxicity assay. Values were normalized to scr control in each setting. **(B, C)** KMM-1 cells were transfected with single (s1, s2, s3) or pooled siRNAs and 48h later (B) mRNA expression levels were determined by qPCR where the results are presented in terms of fold change after normalizing to β-actin mRNA and (C) protein levels were measured via western blot analysis where the Sodium-Potassium ATPase was used as housekeeping gene. **(D)** Live cell-imaging analysis. Tumor cells were transfected with siCAMK1D or scr siRNA sequences and co-cultured with MILs. A fluorescent dye (YOYO-1) was added as an indicator of apoptosis and the graph shows the green object counted (GCO). The experiment is representative of three independent experiments. Right: Representative pictures from the live-cell microscopy. Top: siCAMK1D transfected KMM-1 cells with the addition of MILs. Bottom: scr-transfected KMM-1 cells with the addition of MILs.

YOYO-1 was added in the co-culture to detect apoptotic cells. Apoptotic cells are indicated by the green color. **(E)** Luciferase-based killing assay for detection of T cell-mediated cytotoxicity in the presence of the indicated concentrations of anti-MHC-I antibody (red line) and IgG2a isotype as positive control (black line). Anti-MHC-I antibody was added to KMM-1 cells in the absence of T cells as negative control (grey line). **(F)** KMM-1-luc were pulsed with 0,005µg/ml of HLA-A*02 matched flu peptide for 1h before co-culture with flu-specific T cells or medium control (viability setting) for 20h. T cell-mediated lysis or viability impact of target knockdown was measured by luciferase assay. **(G)** End-point PCR analysis of CAMK1D expression in U266 cells. KMM-1 cells were used as positive control. β-actin was used as housekeeping gene. H_2O served as no template control. **(H)** Quantitative PCR (qPCR) showing CAMK1D knockdown efficiency in KMM-1 and U266 cell lines. Results are presented in terms of fold change after normalization to β-actin mRNA. **(I)** Live cell-imaging analysis. U266 tumor cells were transfected with siCAMK1D or scr siRNA sequences and co-cultured with MILs. No MILs -condition served as viability control. Tumor cell death was measured by the addition of the YOYO-1 dye. Columns show the green object counted (GCO). **(J)** CAMK1D expression by gene expression profiling (probe set 235626_at) in human MBC, PPC, BMPC, MGUS, MM and HMCL.*; BMPC showed significantly lower CAMK1D expression than PPC, MGUS, MM and HMCL ($p < 0.05$; each). ***; MBC showed significantly higher CAMK1D expression than BMPC, PPC, MGUS, MM and HMCL ($p < 0.001$; each). **(A, B)** Graphs show mean +/- SEM. Cumulative data of at least two independent experiments. **(D)** Graph shows mean +/- SEM. P-value was calculated using paired two-tailed student´s t-test. **(E)** Representative data of at least three independent experiments. Graph shows mean +/- SD. **(F, H, I)** Representative data of at least two independent experiments. Graphs show mean +/- SEM. P-values were calculated using unpaired two-tailed student´s t-test. * $p < 0.05$, ** $p < 0.01$, *** $p < 0.001$, **** $p< 0.0001$

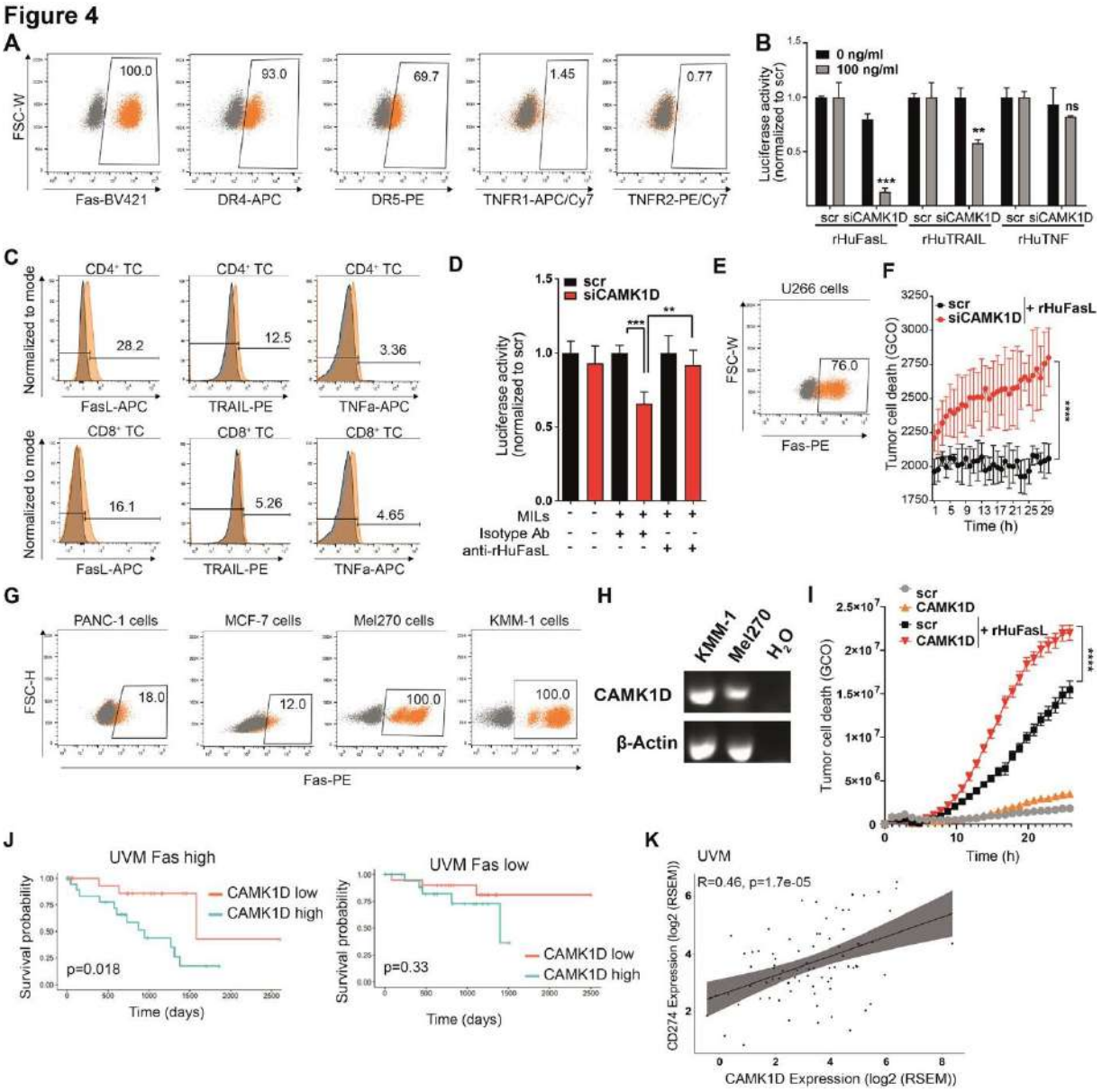

Figure 4. Effect of CAMK1D knockdown in different tumor entities. (A) Representative FACS analysis of Fas, DR4, DR5, TNFR1 and TNFR2 expression in KMM-1 cells. Cell surface expression was measured by flow cytometry. Positive tumor cells are marked in orange while isotype is shown as grey dots. **(B)** KMM-1-luc cells were transfected with scr or CAMK1D siRNAs and treated with recombinant FasL, TRAIL or TNF. Luciferase activity was measured after 20h of treatment. Experiments were performed in triplicates and representative results of three independent experiments are shown. **(C)** Representative FACS analysis of FasL, TRAIL and membrane bound TNFa expression on CD4 and CD8 –positive MILs. Isotype controls are shown as grey histograms. **(D)** Luciferase-based assay: scr or siCAMK1D transfected KMM-1 were co-cultured with MILs in the presence of a FasL neutralizing (anti-FasL) antibody or with an isotype control. Loss of luciferase activity was measured. **(E)** Representative FACS analysis of Fas expression in U266 cells. Positive tumor cells are marked in orange while isotype is shown as grey dots. **(F)** Live cell-imaging analysis. U266 tumor cells were transfected with siCAMK1D or scr siRNA sequences and treated with rHuFasL. The YOYO-1 dye was added as an indicator of tumor cell death. The experiment is representative of three independent experiments and shows the green objects counted (GCO). **(G)** Representative FACS analysis of Fas expression in PANC-1, MCF-7, Mel270 and KMM-1 cells. Tumor cells were stained with conjugated antibodies against Fas. Cell

surface expression was measured by flow cytometry. Positive tumor cells are marked in orange while isotype is shown as grey dots. **(H)** End-point PCR showing CAMK1D expression in the uveal melanoma cell line Mel270. KMM-1 multiple myeloma cells were used as positive control. β-actin was used as housekeeping gene. Water served as no template control. **(I)** Live cell-imaging analysis showing uveal melanoma cells transfected with siCAMK1D or scr siRNA sequence upon exposure to rHuFasL or medium control. A fluorescent dye (YOYO-1) was added as an indicator of apoptosis measured as green object counted (GCO). The experiment is representative of two independent experiments. Values denote mean ± SEM. **(J)** Correlation between CAMK1D and Fas expression on patients´ survival in UVM. Fas high and Fas low UVM patients were divided in CAMK1D high and low expression according to the median of CAMK1D expression. Kaplan-Meier curves showing the correlation between CAMK1D expression and patients' survival probability were generated using TCGA clinical data. Significance was calculated using the log-rank test. **(K)** CAMK1D and PD-L1 correlation is depicted. **(B, D)** Graphs show mean +/- SD. P-values were calculated using unpaired two-tailed student´s t-test. **(F)** Graph shows mean +/- SD. P-value was calculated using paired two-tailed student´s t-test. **(I)** Representative data of at least two independent experiments. Graph shows mean +/- SEM. P-value was calculated using paired two-tailed student´s t-test* $p < 0.05$, ** $p < 0.01$, *** $p < 0.001$, **** $p < 0.0001$

Figure 5

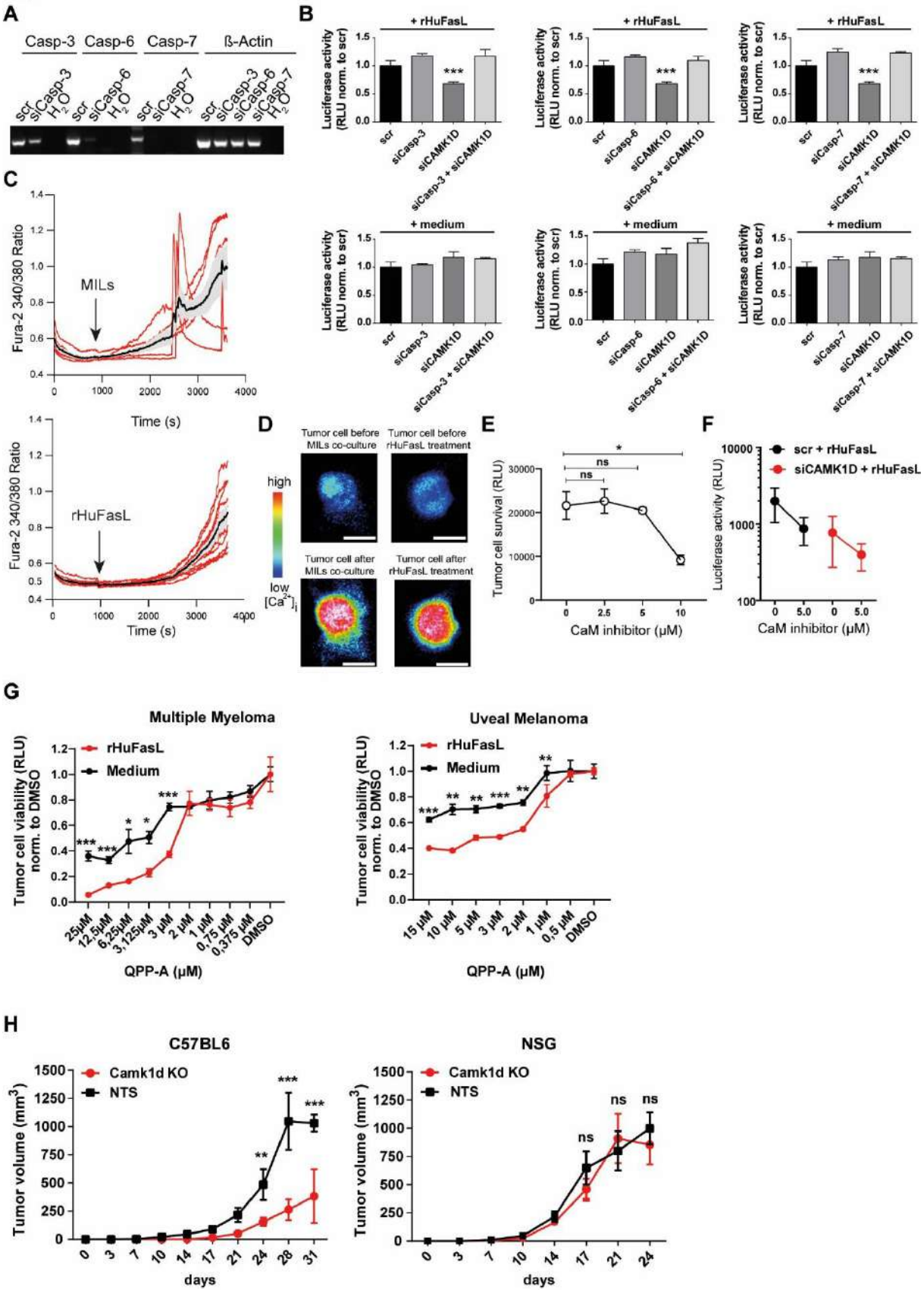
A
Casp-3
Casp-6
Casp-7
ß-Actin
scr
siCasp-3
siCasp-6
siCasp-7
H2O
B
+ rHuFasL
+ medium
Luciferase activity (RLU norm. to scr)
scr
siCasp-3
siCasp-6
siCasp-7
siCAMK1D
siCasp-3 + siCAMK1D
siCasp-6 + siCAMK1D
siCasp-7 + siCAMK1D
C
Fura-2 340/380 Ratio
MILs
rHuFasL
Time (s)
D
Tumor cell before MILs co-culture
Tumor cell before rHuFasL treatment
Tumor cell after MILs co-culture
Tumor cell after rHuFasL treatment
high
low
[Ca2+]i
E
Tumor cell survival (RLU)
CaM inhibitor (µM)
ns
F
scr + rHuFasL
siCAMK1D + rHuFasL
Luciferase activity (RLU)
CaM inhibitor (µM)
G
Multiple Myeloma
Uveal Melanoma
rHuFasL
Medium
Tumor cell viability (RLU) norm. to DMSO
QPP-A (µM)
25µM
12,5µM
6,25µM
3,125µM
3 µM
2 µM
1 µM
0,75 µM
0,375 µM
DMSO
15 µM
10 µM
5 µM
3 µM
2 µM
1 µM
0,5 µM
DMSO
H
C57BL6
NSG
Camk1d KO
NTS
Tumor volume (mm3)
days

Figure 5. CAMK1D regulation. (A) Caspase-3, -6 and -7 expression and knockdown in KMM-1 cells was measured via end-point PCR. **(B)** Effector caspases were knocked down alone or in combination with CAMK1D and stimulated with rHuFasL or with medium control. Luciferase activity was measured after 20h of treatment. Experiments were performed in quadruplicates and representative results of three independent experiments are shown. **(C)** Intracellular calcium response in KMM-1 cells upon (top) MILs co-culture and (bottom) rHuFasL treatment. **(D)** Representative picture of intracellular free Ca^{2+} measurement in KMM-1 scr-transfected cells before (top) and after (bottom) co-culture with MILs or treated with rHuFasL. **(E)** KMM-1 cells were treated with different concentrations of CaM inhibitor (W-7 hydrochloride) and tumor cell survival was measured by luciferase intensity. **(F)** scr and siCAMK1D KMM-1 transfected cells were treated with rHuFasL together with the indicated concentration of CaM inhibitor. **(G)** KMM-1 (left) and Mel270 (right) cells were treated with the indicated concentration of CAMK1D inhibitor (QPP-A) and exposed to rHuFasL or medium. Tumor cell survival was measured by luciferase intensity. **(H)** C57BL6 (n=12) and NOD/SCID gamma chain (NSG) mice (n=12) were s.c injected with 1 x 10^5 MC38 Camk1d KO and MC38 NTS cells each into the right and left flank of one mouse, respectively. Tumor growth was measured twice a week. Graphs show mean ± SEM and statistical significance was calculated using two-way ANOVA Bonferroni post test. **(B)** Graphs show mean ± SD. Statistical significance was calculated using unpaired, two-tailed Student's t-test. **(E, F, G)** Experiments were performed in triplicates and representative results of three independent experiments are shown. Graphs show mean ± SEM and statistical significance was calculated using unpaired, two-tailed Student's t-test. * $p \leq 0.05$; ** $p \leq 0.01$; *** $p \leq 0.001$; **** $p \leq 0.0001$.

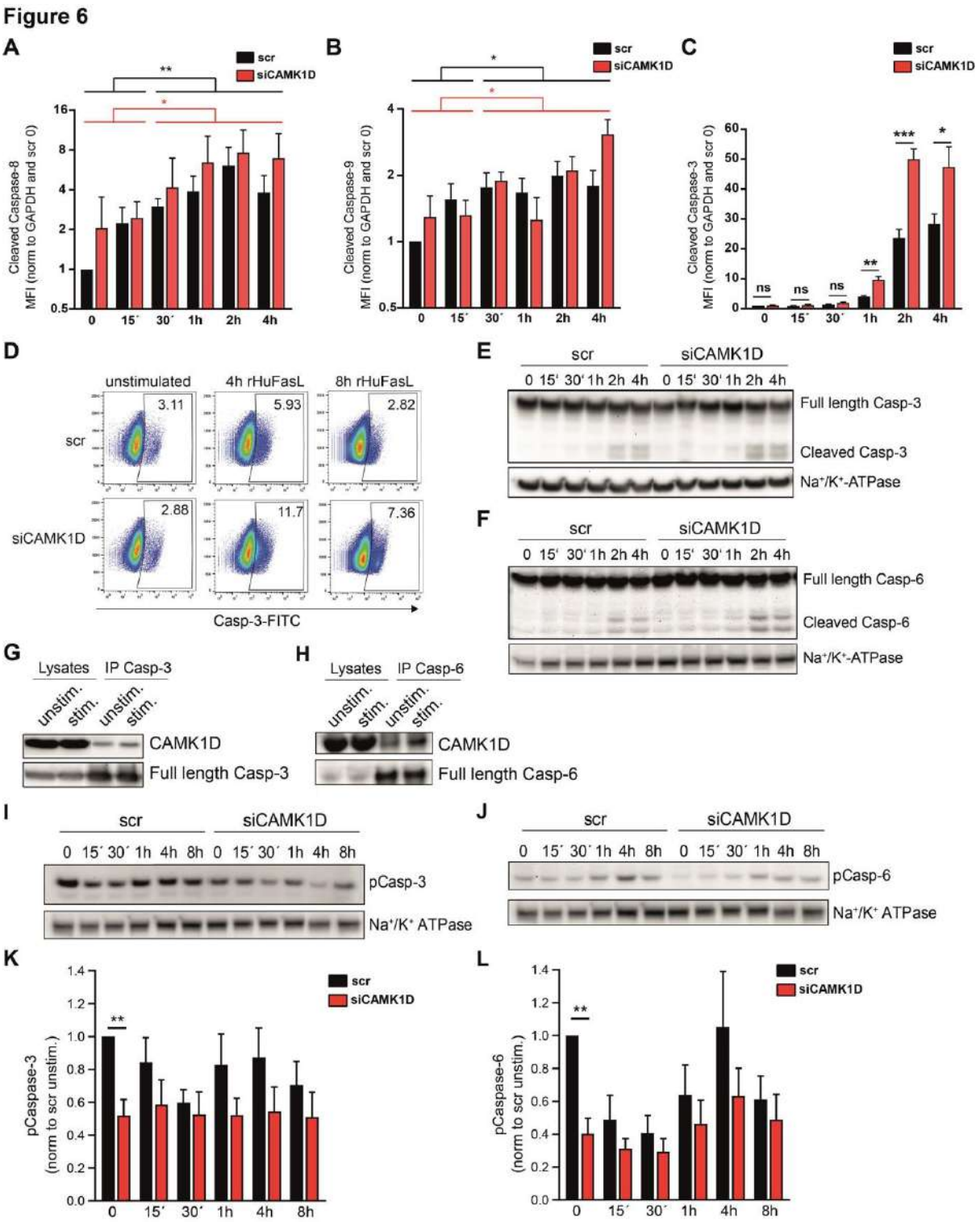

Figure 6. Pathways regulated by CAMK1D. (A-C) Luminex assays measuring apoptosis proteins. CAMK1D-proficient and -deficient cells were stimulated with rHuFasL for the indicated time frames. Protein levels were normalized to GAPDH and compared to scr-unstimulated cells. The amount of (A) cleaved caspase-8 (B) cleaved caspase-9 and (C) cleaved caspase-3 was measured. Graphs show cumulative data of at

least two independent experiments. **(D)** FACS analysis of scr and siCAMK1D transfected KMM-1 cells treated for the given time frames with rHuFasL. Gate marks active caspase-3 labeled cells. **(E, F)** KMM-1 cells were treated as in (A-C) and full-length and cleaved **(E)** caspase-3 and **(F)** caspase-6 were measured via western blot. The Sodium-Potassium ATPase was used as housekeeping gene. Representative results of at least two independent experiments. **(G, H)** Representative blots showing co-immunoprecipitation of (G) caspase-3 and CAMK1D, (H) caspase-6 and CAMK1D. KMM-1 cells were stimulated with rHuFasL for 4h. Unstimulated cells were used as negative control. Unstimulated and stimulated cell lysates were used as positive control for CAMK1D detection. **(I, J)** Western blot measuring phosphorylated caspase-3 and caspase-6 upon rHuFasL stimulation. The Sodium-Potassium ATPase was used as housekeeping gene. **(K, L)** Quantification of (K) phosphorylated caspase-3 and (L) phosphorylated caspase-6 upon rHuFasL stimulation for the indicated time frames. Graphs show cumulative data of four independent experiments. **(A, B, K, L)** Graphs show mean ± SEM and statistical significance was calculated using unpaired, two-tailed Student's t-test. **(C)** Graph shows mean ± SD and statistical significance was calculated using unpaired, two-tailed Student's t-test. * $p \leq 0.05$; ** $p \leq 0.01$; *** $p \leq 0.001$; **** $p \leq 0.0001$.

References

1. Choi C, Witzens M, Bucur M, Feuerer M, Sommerfeldt N, Trojan A, Ho A, Schirrmacher V, Goldschmidt H, and Beckhove P. Enrichment of functional CD8 memory T cells specific for MUC1 in bone marrow of patients with multiple myeloma. *Blood.* 2005;105(5):2132-4.
2. Safi S, Yamauchi Y, Rathinasamy A, Stamova S, Eichhorn M, Warth A, Rauch G, Dienemann H, Hoffmann H, and Beckhove P. Functional T cells targeting tumor-associated antigens are predictive for recurrence-free survival of patients with radically operated non-small cell lung cancer. *Oncoimmunology.* 2017;6(11):e1360458.
3. Schmitz-Winnenthal FH, Volk C, Z'Graggen K, Galindo L, Nummer D, Ziouta Y, Bucur M, Weitz J, Schirrmacher V, Buchler MW, et al. High frequencies of functional tumor-reactive T cells in bone marrow and blood of pancreatic cancer patients. *Cancer research.* 2005;65(21):10079-87.
4. Galon J, Costes A, Sanchez-Cabo F, Kirilovsky A, Mlecnik B, Lagorce-Pages C, Tosolini M, Camus M, Berger A, Wind P, et al. Type, density, and location of immune cells within human colorectal tumors predict clinical outcome. *Science.* 2006;313(5795):1960-4.
5. Reissfelder C, Stamova S, Gossmann C, Braun M, Bonertz A, Walliczek U, Grimm M, Rahbari NN, Koch M, Saadati M, et al. Tumor-specific cytotoxic T lymphocyte activity determines colorectal cancer patient prognosis. *J Clin Invest.* 2015;125(2):739-51.
6. Abiko K, Matsumura N, Hamanishi J, Horikawa N, Murakami R, Yamaguchi K, Yoshioka Y, Baba T, Konishi I, and Mandai M. IFN-gamma from lymphocytes induces PD-L1 expression and promotes progression of ovarian cancer. *British journal of cancer.* 2015;112(9):1501-9.
7. Alsaab HO, Sau S, Alzhrani R, Tatiparti K, Bhise K, Kashaw SK, and Iyer AK. PD-1 and PD-L1 Checkpoint Signaling Inhibition for Cancer Immunotherapy: Mechanism, Combinations, and Clinical Outcome. *Frontiers in pharmacology.* 2017;8(561.
8. Zou W, Wolchok JD, and Chen L. PD-L1 (B7-H1) and PD-1 pathway blockade for cancer therapy: Mechanisms, response biomarkers, and combinations. *Sci Transl Med.* 2016;8(328):328rv4.
9. Hodi FS, O'Day SJ, McDermott DF, Weber RW, Sosman JA, Haanen JB, Gonzalez R, Robert C, Schadendorf D, Hassel JC, et al. Improved survival with ipilimumab in patients with metastatic melanoma. *N Engl J Med.* 2010;363(8):711-23.
10. Slovin SF, Higano CS, Hamid O, Tejwani S, Harzstark A, Alumkal JJ, Scher HI, Chin K, Gagnier P, McHenry MB, et al. Ipilimumab alone or in combination with radiotherapy in metastatic castration-resistant prostate cancer: results from an open-label, multicenter phase I/II study. *Ann Oncol.* 2013;24(7):1813-21.
11. Yang JC, Hughes M, Kammula U, Royal R, Sherry RM, Topalian SL, Suri KB, Levy C, Allen T, Mavroukakis S, et al. Ipilimumab (anti-CTLA4 antibody) causes regression of metastatic renal cell cancer associated with enteritis and hypophysitis. *J Immunother.* 2007;30(8):825-30.
12. Topalian SL, Hodi FS, Brahmer JR, Gettinger SN, Smith DC, McDermott DF, Powderly JD, Carvajal RD, Sosman JA, Atkins MB, et al. Safety, activity, and immune correlates of anti-PD-1 antibody in cancer. *N Engl J Med.* 2012;366(26):2443-54.
13. Bu X, Mahoney KM, and Freeman GJ. Learning from PD-1 Resistance: New Combination Strategies. *Trends Mol Med.* 2016;22(6):448-51.
14. Carbognin L, Pilotto S, Milella M, Vaccaro V, Brunelli M, Calio A, Cuppone F, Sperduti I, Giannarelli D, Chilosi M, et al. Differential Activity of Nivolumab, Pembrolizumab and MPDL3280A according to the Tumor Expression of Programmed Death-Ligand-1 (PD-L1): Sensitivity Analysis of Trials in Melanoma, Lung and Genitourinary Cancers. *PLoS One.* 2015;10(6):e0130142.
15. Hugo W, Zaretsky JM, Sun L, Song C, Moreno BH, Hu-Lieskovan S, Berent-Maoz B, Pang J, Chmielowski B, Cherry G, et al. Genomic and Transcriptomic Features of Response to Anti-PD-1 Therapy in Metastatic Melanoma. *Cell.* 2016;165(1):35-44.
16. Nowicki TS, Hu-Lieskovan S, and Ribas A. Mechanisms of Resistance to PD-1 and PD-L1 Blockade. *Cancer journal.* 2018;24(1):47-53.
17. Fourcade J, Sun Z, Benallaoua M, Guillaume P, Luescher IF, Sander C, Kirkwood JM, Kuchroo V, and Zarour HM. Upregulation of Tim-3 and PD-1 expression is associated with tumor antigen-specific CD8+ T cell dysfunction in melanoma patients. *J Exp Med.* 2010;207(10):2175-86.

18. Wang L, Rubinstein R, Lines JL, Wasiuk A, Ahonen C, Guo Y, Lu LF, Gondek D, Wang Y, Fava RA, et al. VISTA, a novel mouse Ig superfamily ligand that negatively regulates T cell responses. *The Journal of experimental medicine.* 2011;208(3):577-92.
19. Jing W, Gershan JA, Weber J, Tlomak D, McOlash L, Sabatos-Peyton C, and Johnson BD. Combined immune checkpoint protein blockade and low dose whole body irradiation as immunotherapy for myeloma. *J Immunother Cancer.* 2015;3(1):2.
20. Hallett WH, Jing W, Drobyski WR, and Johnson BD. Immunosuppressive effects of multiple myeloma are overcome by PD-L1 blockade. *Biol Blood Marrow Transplant.* 2011;17(8):1133-45.
21. Benson DM, Jr., Bakan CE, Mishra A, Hofmeister CC, Efebera Y, Becknell B, Baiocchi RA, Zhang J, Yu J, Smith MK, et al. The PD-1/PD-L1 axis modulates the natural killer cell versus multiple myeloma effect: a therapeutic target for CT-011, a novel monoclonal anti-PD-1 antibody. *Blood.* 2010;116(13):2286-94.
22. Tamura H, Ishibashi M, Yamashita T, Tanosaki S, Okuyama N, Kondo A, Hyodo H, Shinya E, Takahashi H, Dong H, et al. Marrow stromal cells induce B7-H1 expression on myeloma cells, generating aggressive characteristics in multiple myeloma. *Leukemia.* 2013;27(2):464-72.
23. Lesokhin AM, Ansell SM, Armand P, Scott EC, Halwani A, Gutierrez M, Millenson MM, Cohen AD, Schuster SJ, Lebovic D, et al. Nivolumab in Patients With Relapsed or Refractory Hematologic Malignancy: Preliminary Results of a Phase Ib Study. *J Clin Oncol.* 2016;34(23):2698-704.
24. Sonneveld P, Schmidt-Wolf IG, van der Holt B, El Jarari L, Bertsch U, Salwender H, Zweegman S, Vellenga E, Broyl A, Blau IW, et al. Bortezomib induction and maintenance treatment in patients with newly diagnosed multiple myeloma: results of the randomized phase III HOVON-65/ GMMG-HD4 trial. *J Clin Oncol.* 2012;30(24):2946-55.
25. Hulin C, Belch A, Shustik C, Petrucci MT, Duhrsen U, Lu J, Song K, Rodon P, Pegourie B, Garderet L, et al. Updated Outcomes and Impact of Age With Lenalidomide and Low-Dose Dexamethasone or Melphalan, Prednisone, and Thalidomide in the Randomized, Phase III FIRST Trial. *J Clin Oncol.* 2016.
26. Lokhorst HM, Plesner T, Laubach JP, Nahi H, Gimsing P, Hansson M, Minnema MC, Lassen U, Krejcik J, Palumbo A, et al. Targeting CD38 with Daratumumab Monotherapy in Multiple Myeloma. *N Engl J Med.* 2015;373(13):1207-19.
27. Child JA, Morgan GJ, Davies FE, Owen RG, Bell SE, Hawkins K, Brown J, Drayson MT, and Selby PJ. High-Dose Chemotherapy with Hematopoietic Stem-Cell Rescue for Multiple Myeloma. *N Engl J Med.* 2003;348(19):1875-83.
28. Seckinger A, Delgado JA, Moser S, Moreno L, Neuber B, Grab A, Lipp S, Merino J, Prosper F, Emde M, et al. Target Expression, Generation, Preclinical Activity, and Pharmacokinetics of the BCMA-T Cell Bispecific Antibody EM801 for Multiple Myeloma Treatment. *Cancer cell.* 2017;31(3):396-410.
29. Greipp PR, Miguel JS, Durie BGM, Crowley JJ, Barlogie B, Bladé J, Boccadoro M, Child JA, Avet-Loiseau H, Harousseau J-L, et al. International staging system for multiple myeloma. *J Clin Oncol.* 2005;23(15):3412-20.
30. Durie BG. Staging and kinetics of multiple myeloma. *Semin Oncol.* 1986;13(3):300-9.
31. Blade J, Samson D, Reece D, Apperley J, Bjorkstrand B, Gahrton G, Gertz M, Giralt S, Jagannath S, and Vesole D. Criteria for evaluating disease response and progression in patients with multiple myeloma treated by high-dose therapy and haemopoietic stem cell transplantation. Myeloma Subcommittee of the EBMT. European Group for Blood and Marrow Transplant. *Br J Haematol.* 1998;102(5):1115-23.
32. Seckinger A, Delgado JA, Moser S, Moreno L, Neuber B, Grab A, Lipp S, Merino J, Prosper F, Emde M, et al. Target Expression, Generation, Preclinical Activity, and Pharmacokinetics of the BCMA-T Cell Bispecific Antibody EM801 for Multiple Myeloma Treatment. *Cancer Cell.* 2017;31(3):396-410.
33. Hose D, Moreaux J, Meissner T, Seckinger A, Goldschmidt H, Benner A, Mahtouk K, Hillengass J, Rème T, Vos JD, et al. Induction of angiogenesis by normal and malignant plasma cells. *Blood.* 2009;114(1):128-43.
34. Moreaux J, Cremer FW, Reme T, Raab M, Mahtouk K, Kaukel P, Pantesco V, Vos JD, Jourdan E, Jauch A, et al. The level of TACI gene expression in myeloma cells is associated with a signature of microenvironment dependence versus a plasmablastic signature. *Blood.* 2005;106(3):1021-30.
35. Zhang XG, Gaillard JP, Robillard N, Lu ZY, Gu ZJ, Jourdan M, Boiron JM, Bataille R, and Klein B. Reproducible obtaining of human myeloma cell lines as a model for tumor stem cell study in human multiple myeloma. *Blood.* 1994;83(12):3654-63.
36. Corre J, Mahtouk K, Attal M, Gadelorge M, Huynh A, Fleury-Cappellesso S, Danho C, Laharrague P, Klein B, Rème T, et al. Bone marrow mesenchymal stem cells are abnormal in multiple myeloma. *Leukemia.* 2007;21(5):1079-88.

37. Fuhler GM, Baanstra M, Chesik D, Somasundaram R, Seckinger A, Hose D, Peppelenbosch MP, and Bos NA. Bone marrow stromal cell interaction reduces syndecan-1 expression and induces kinomic changes in myeloma cells. *Exp Cell Res.* 2010;316(11):1816-28.
38. Griewank KG, Yu X, Khalili J, Sozen MM, Stempke-Hale K, Bernatchez C, Wardell S, Bastian BC, and Woodman SE. Genetic and molecular characterization of uveal melanoma cell lines. *Pigment cell & melanoma research.* 2012;25(2):182-7.
39. Dudley ME, Wunderlich JR, Shelton TE, Even J, and Rosenberg SA. Generation of tumor-infiltrating lymphocyte cultures for use in adoptive transfer therapy for melanoma patients. *Journal of Immunotherapy.* 2003;26(4):332-42.
40. Jin J, Sabatino M, Somerville R, Wilson JR, Dudley ME, Stroncek DF, and Rosenberg SA. Simplified method of the growth of human tumor infiltrating lymphocytes in gas-permeable flasks to numbers needed for patient treatment. *J Immunother.* 2012;35(3):283-92.
41. Hose D, Reme T, Hielscher T, Moreaux J, Meissner T, Seckinger A, Benner A, Shaughnessy JD, Barlogie B, Zhou Y, et al. Proliferation is a central independent prognostic factor and target for personalized and risk adapted treatment in multiple myeloma. *Haematologica.* 2011;96(87-95.
42. Seckinger A, Meißner T, Moreaux J, Depeweg D, Hillengass J, Hose K, Reme T, Rosen-Wolff A, Jauch A, Schnettler R, et al. Clinical and prognostic role of annexin A2 in multiple myeloma. *Blood.* 2012;120(5):1087-94.
43. Wan YW, Allen GI, and Liu Z. TCGA2STAT: simple TCGA data access for integrated statistical analysis in R. *Bioinformatics.* 2016;32(6):952-4.
44. Gilbert DF, Erdmann G, Zhang X, Fritzsche A, Demir K, Jaedicke A, Muehlenberg K, Wanker EE, and Boutros M. A novel multiplex cell viability assay for high-throughput RNAi screening. *PLoS One.* 2011;6(12):e28338.
45. Khandelwal N, Breinig M, Speck T, Michels T, Kreutzer C, Sorrentino A, Sharma AK, Umansky L, Conrad H, Poschke I, et al. A high-throughput RNAi screen for detection of immune-checkpoint molecules that mediate tumor resistance to cytotoxic T lymphocytes. *EMBO Mol Med.* 2015;7(4):450-63.
46. Boutros M, Bras LP, and Huber W. Analysis of cell-based RNAi screens. *Genome Biol.* 2006;7(7):R66.
47. Zhang C, Xin H, Zhang W, Yazaki PJ, Zhang Z, Le K, Li W, Lee H, Kwak L, Forman S, et al. CD5 Binds to Interleukin-6 and Induces a Feed-Forward Loop with the Transcription Factor STAT3 in B Cells to Promote Cancer. *Immunity.* 2016;44(4):913-23.
48. Tiedemann RE, Zhu YX, Schmidt J, Yin H, Shi CX, Que Q, Basu G, Azorsa D, Perkins LM, Braggio E, et al. Kinome-wide RNAi studies in human multiple myeloma identify vulnerable kinase targets, including a lymphoid-restricted kinase, GRK6. *Blood.* 2010;115(8):1594-604.
49. Ye DZ, and Field J. PAK signaling in cancer. *Cell Logist.* 2012;2(2):105-16.
50. Algazi AP, Tsai KK, Shoushtari AN, Munhoz RR, Eroglu Z, Piulats JM, Ott PA, Johnson DB, Hwang J, Daud AI, et al. Clinical outcomes in metastatic uveal melanoma treated with PD-1 and PD-L1 antibodies. *Cancer.* 2016;122(21):3344-53.
51. Elnemr A, Ohta T, Yachie A, Kayahara M, Kitagawa H, Fujimura T, Ninomiya I, Fushida S, Nishimura GI, Shimizu K, et al. Human pancreatic cancer cells disable function of Fas receptors at several levels in Fas signal transduction pathway. *International journal of oncology.* 2001;18(2):311-6.
52. Elnemr A, Ohta T, Yachie A, Kayahara M, Kitagawa H, Ninomiya I, Fushida S, Fujimura T, Nishimura G, Shimizu K, et al. Human pancreatic cancer cells express non-functional Fas receptors and counterattack lymphocytes by expressing Fas ligand; a potential mechanism for immune escape. *International journal of oncology.* 2001;18(1):33-9.
53. Sakagami H, Kamata A, Nishimura H, Kasahara J, Owada Y, Takeuchi Y, Watanabe M, Fukunaga K, and Kondo H. Prominent expression and activity-dependent nuclear translocation of Ca2+/calmodulin-dependent protein kinase Idelta in hippocampal neurons. *Eur J Neurosci.* 2005;22(11):2697-707.
54. Wozniak AL, Wang X, Stieren ES, Scarbrough SG, Elferink CJ, and Boehning D. Requirement of biphasic calcium release from the endoplasmic reticulum for Fas-mediated apoptosis. *J Cell Biol.* 2006;175(5):709-14.
55. Swulius MT, and Waxham MN. Ca(2+)/calmodulin-dependent protein kinases. *Cell Mol Life Sci.* 2008;65(17):2637-57.
56. McIlwain DR, Berger T, and Mak TW. Caspase functions in cell death and disease. *Cold Spring Harb Perspect Biol.* 2013;5(4):a008656.
57. Parrish AB, Freel CD, and Kornbluth S. Cellular mechanisms controlling caspase activation and function. *Cold Spring Harb Perspect Biol.* 2013;5(6).

58. Alvarado-Kristensson M, Melander F, Leandersson K, Ronnstrand L, Wernstedt C, and Andersson T. p38-MAPK signals survival by phosphorylation of caspase-8 and caspase-3 in human neutrophils. *J Exp Med.* 2004;199(4):449-58.
59. Suzuki A, Kusakai G, Kishimoto A, Shimojo Y, Miyamoto S, Ogura T, Ochiai A, and Esumi H. Regulation of caspase-6 and FLIP by the AMPK family member ARK5. *Oncogene.* 2004;23(42):7067-75.
60. Alvarado-Kristensson M, and Andersson T. Protein phosphatase 2A regulates apoptosis in neutrophils by dephosphorylating both p38 MAPK and its substrate caspase 3. *J Biol Chem.* 2005;280(7):6238-44.
61. Bergamaschi A, Kim YH, Kwei KA, La Choi Y, Bocanegra M, Langerod A, Han W, Noh DY, Huntsman DG, Jeffrey SS, et al. CAMK1D amplification implicated in epithelial-mesenchymal transition in basal-like breast cancer. *Mol Oncol.* 2008;2(4):327-39.
62. Ashkenazi A. Targeting the extrinsic apoptosis pathway in cancer. *Cytokine Growth Factor Rev.* 2008;19(3-4):325-31.
63. Green DR, and Ferguson TA. The role of Fas ligand in immune privilege. *Nat Rev Mol Cell Biol.* 2001;2(12):917-24.
64. Kischkel FC, Hellbardt S, Behrmann I, Germer M, Pawlita M, Krammer PH, and Peter ME. Cytotoxicity-dependent APO-1 (Fas/CD95)-associated proteins form a death-inducing signaling complex (DISC) with the receptor. *EMBO J.* 1995;14(22):5579-88.
65. Mellier G, Huang S, Shenoy K, and Pervaiz S. TRAILing death in cancer. *Mol Aspects Med.* 2010;31(1):93-112.
66. Lavrik I, Krueger A, Schmitz I, Baumann S, Weyd H, Krammer PH, and Kirchhoff S. The active caspase-8 heterotetramer is formed at the CD95 DISC. *Cell Death Differ.* 2003;10(1):144-5.
67. Nicholson DW, Ali A, Thornberry NA, Vaillancourt JP, Ding CK, Gallant M, Gareau Y, Griffin PR, Labelle M, Lazebnik YA, et al. Identification and inhibition of the ICE/CED-3 protease necessary for mammalian apoptosis. *Nature.* 1995;376(6535):37-43.
68. Powley IR, Hughes MA, Cain K, and MacFarlane M. Caspase-8 tyrosine-380 phosphorylation inhibits CD95 DISC function by preventing procaspase-8 maturation and cycling within the complex. *Oncogene.* 2016;35(43):5629-40.
69. Irmler M, Thome M, Hahne M, Schneider P, Hofmann K, Steiner V, Bodmer JL, Schroter M, Burns K, Mattmann C, et al. Inhibition of death receptor signals by cellular FLIP. *Nature.* 1997;388(6638):190-5.
70. Pistritto G, Trisciuoglio D, Ceci C, Garufi A, and D'Orazi G. Apoptosis as anticancer mechanism: function and dysfunction of its modulators and targeted therapeutic strategies. *Aging.* 2016;8(4):603-19.
71. Pepper C, Hoy T, and Bentley DP. Bcl-2/Bax ratios in chronic lymphocytic leukaemia and their correlation with in vitro apoptosis and clinical resistance. *British journal of cancer.* 1997;76(7):935-8.
72. Soengas MS, Capodieci P, Polsky D, Mora J, Esteller M, Opitz-Araya X, McCombie R, Herman JG, Gerald WL, Lazebnik YA, et al. Inactivation of the apoptosis effector Apaf-1 in malignant melanoma. *Nature.* 2001;409(6817):207-11.
73. Berthelet J, and Dubrez L. Regulation of Apoptosis by Inhibitors of Apoptosis (IAPs). *Cells.* 2013;2(1):163-87.
74. Marivin A, Berthelet J, Plenchette S, and Dubrez L. The Inhibitor of Apoptosis (IAPs) in Adaptive Response to Cellular Stress. *Cells.* 2012;1(4):711-37.
75. Chen X, Duan N, Zhang C, and Zhang W. Survivin and Tumorigenesis: Molecular Mechanisms and Therapeutic Strategies. *J Cancer.* 2016;7(3):314-23.
76. LaCasse EC, Mahoney DJ, Cheung HH, Plenchette S, Baird S, and Korneluk RG. IAP-targeted therapies for cancer. *Oncogene.* 2008;27(48):6252-75.
77. Cuadrado A, and Nebreda AR. Mechanisms and functions of p38 MAPK signalling. *The Biochemical journal.* 2010;429(3):403-17.
78. Sun X, Gao L, Chien HY, Li WC, and Zhao J. The regulation and function of the NUAK family. *Journal of molecular endocrinology.* 2013;51(2):R15-22.
79. Suzuki A, Kusakai G, Kishimoto A, Lu J, Ogura T, and Esumi H. ARK5 suppresses the cell death induced by nutrient starvation and death receptors via inhibition of caspase 8 activation, but not by chemotherapeutic agents or UV irradiation. *Oncogene.* 2003;22(40):6177-82.
80. Bellucci R, Nguyen HN, Martin A, Heinrichs S, Schinzel AC, Hahn WC, and Ritz J. Tyrosine kinase pathways modulate tumor susceptibility to natural killer cells. *J Clin Invest.* 2012;122(7):2369-83.
81. Dunn GP, Sheehan KC, Old LJ, and Schreiber RD. IFN unresponsiveness in LNCaP cells due to the lack of JAK1 gene expression. *Cancer Res.* 2005;65(8):3447-53.

82. Parampalli Yajnanarayana S, Stubig T, Cornez I, Alchalby H, Schonberg K, Rudolph J, Triviai I, Wolschke C, Heine A, Brossart P, et al. JAK1/2 inhibition impairs T cell function in vitro and in patients with myeloproliferative neoplasms. *Br J Haematol.* 2015;169(6):824-33.
83. Schonberg K, Rudolph J, Vonnahme M, Parampalli Yajnanarayana S, Cornez I, Hejazi M, Manser AR, Uhrberg M, Verbeek W, Koschmieder S, et al. JAK Inhibition Impairs NK Cell Function in Myeloproliferative Neoplasms. *Cancer Res.* 2015;75(11):2187-99.

Figure 1

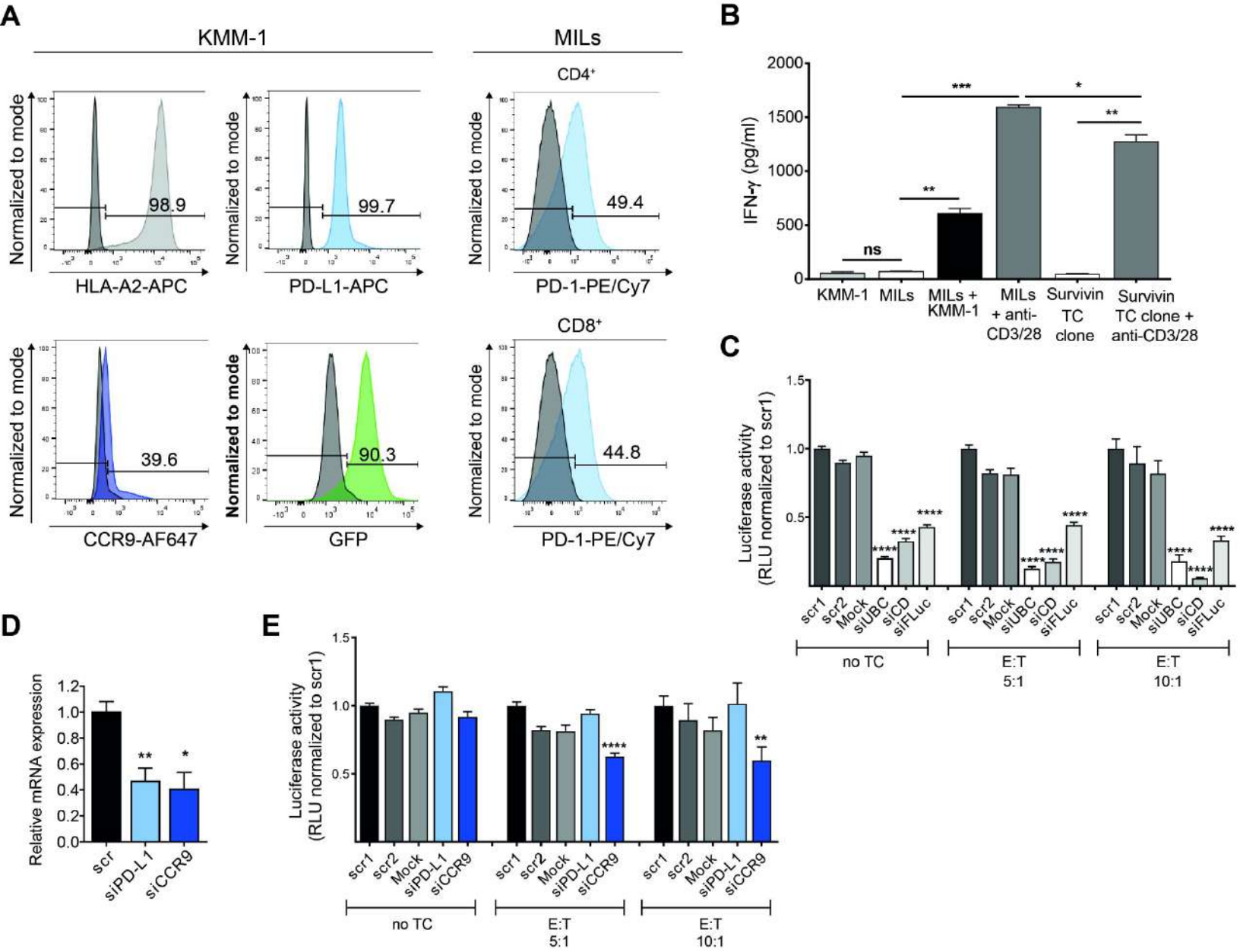
A
KMM-1
MILs
CD4+
CD8+
Normalized to mode
98.9
HLA-A2-APC
99.7
PD-L1-APC
49.4
PD-1-PE/Cy7
39.6
CCR9-AF647
90.3
GFP
44.8
PD-1-PE/Cy7
B
IFN-γ (pg/ml)
2000
1500
1000
500
0
ns
**
***
*
**
KMM-1
MILs
MILs + KMM-1
MILs + anti-CD3/28
Survivin TC clone
Survivin TC clone + anti-CD3/28
C
Luciferase activity (RLU normalized to scr1)
1.5
1.0
0.5
scr1
scr2
Mock
siUBC
siCD
siFLuc
no TC
E:T 5:1
E:T 10:1
D
Relative mRNA expression
1.2
1.0
0.8
0.6
0.4
0.2
0.0
**
*
scr
siPD-L1
siCCR9
E
Luciferase activity (RLU normalized to scr1)
1.5
1.0
0.5
****
**
scr1
scr2
Mock
siPD-L1
siCCR9
no TC
E:T 5:1
E:T 10:1

Figure 2

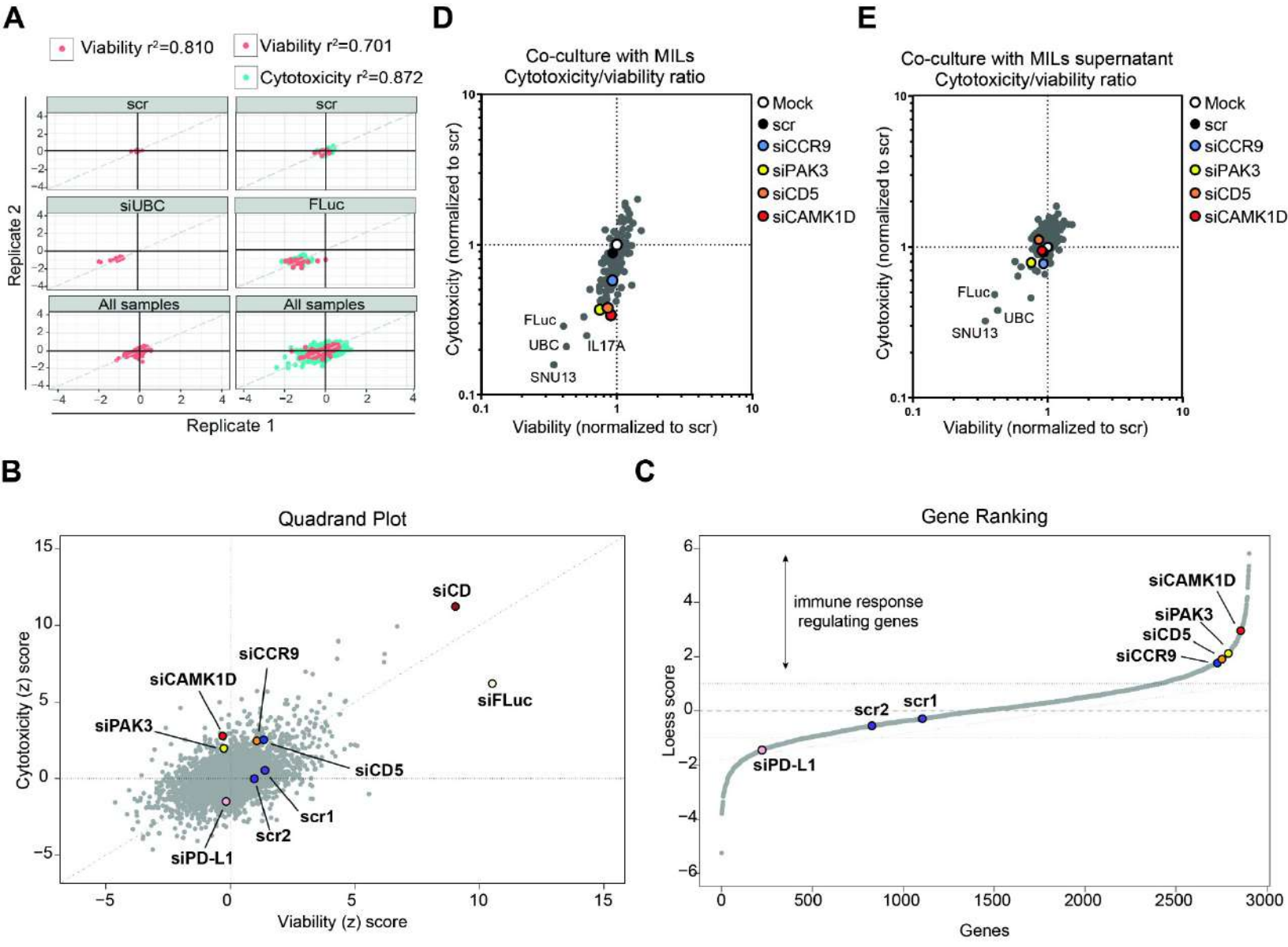
A
Viability r²=0.810
Viability r²=0.701
Cytotoxicity r²=0.872
scr
siUBC
FLuc
All samples
Replicate 2
Replicate 1
D
Co-culture with MILs
Cytotoxicity/viability ratio
Cytotoxicity (normalized to scr)
Viability (normalized to scr)
Mock
scr
siCCR9
siPAK3
siCD5
siCAMK1D
FLuc
UBC
IL17A
SNU13
E
Co-culture with MILs supernatant
Cytotoxicity/viability ratio
B
Quadrand Plot
Cytotoxicity (z) score
Viability (z) score
siCD
siFLuc
siCCR9
siCAMK1D
siPAK3
siCD5
scr1
scr2
siPD-L1
C
Gene Ranking
Loess score
Genes
immune response
regulating genes

Figure 3

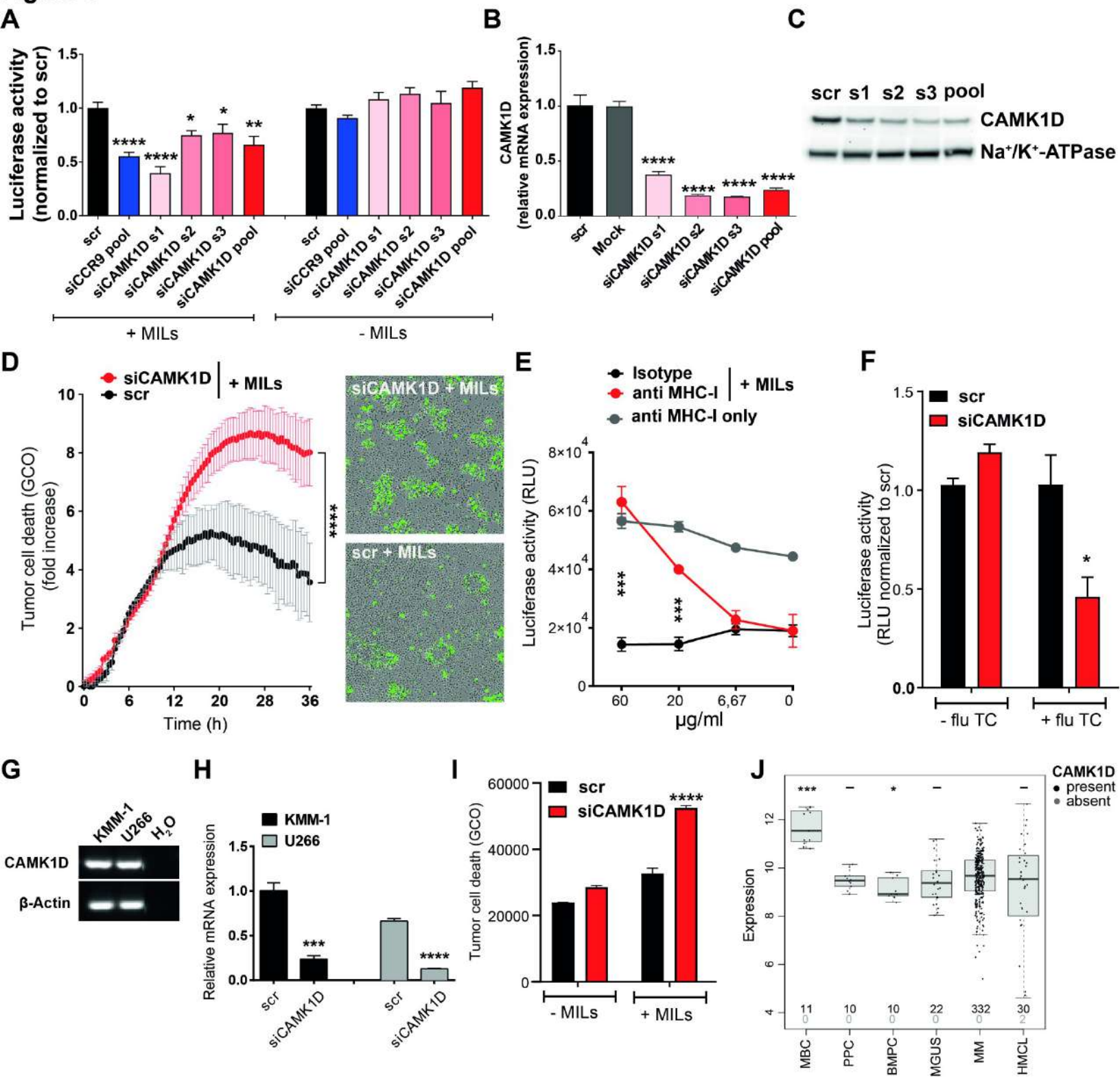
A
Luciferase activity (normalized to scr)
scr
siCCR9 pool
siCAMK1D s1
siCAMK1D s2
siCAMK1D s3
siCAMK1D pool
+ MILs
- MILs
B
CAMK1D (relative mRNA expression)
Mock
C
scr s1 s2 s3 pool
CAMK1D
Na+/K+-ATPase
D
siCAMK1D
scr
+ MILs
Tumor cell death (GCO) (fold increase)
Time (h)
siCAMK1D + MILs
scr + MILs
E
Isotype
anti MHC-I
anti MHC-I only
Luciferase activity (RLU)
µg/ml
F
Luciferase activity (RLU normalized to scr)
- flu TC
+ flu TC
G
KMM-1
U266
H2O
CAMK1D
β-Actin
H
Relative mRNA expression
I
Tumor cell death (GCO)
J
CAMK1D
present
absent
Expression
MBC
PPC
BMPC
MGUS
MM
HMCL

Figure 4

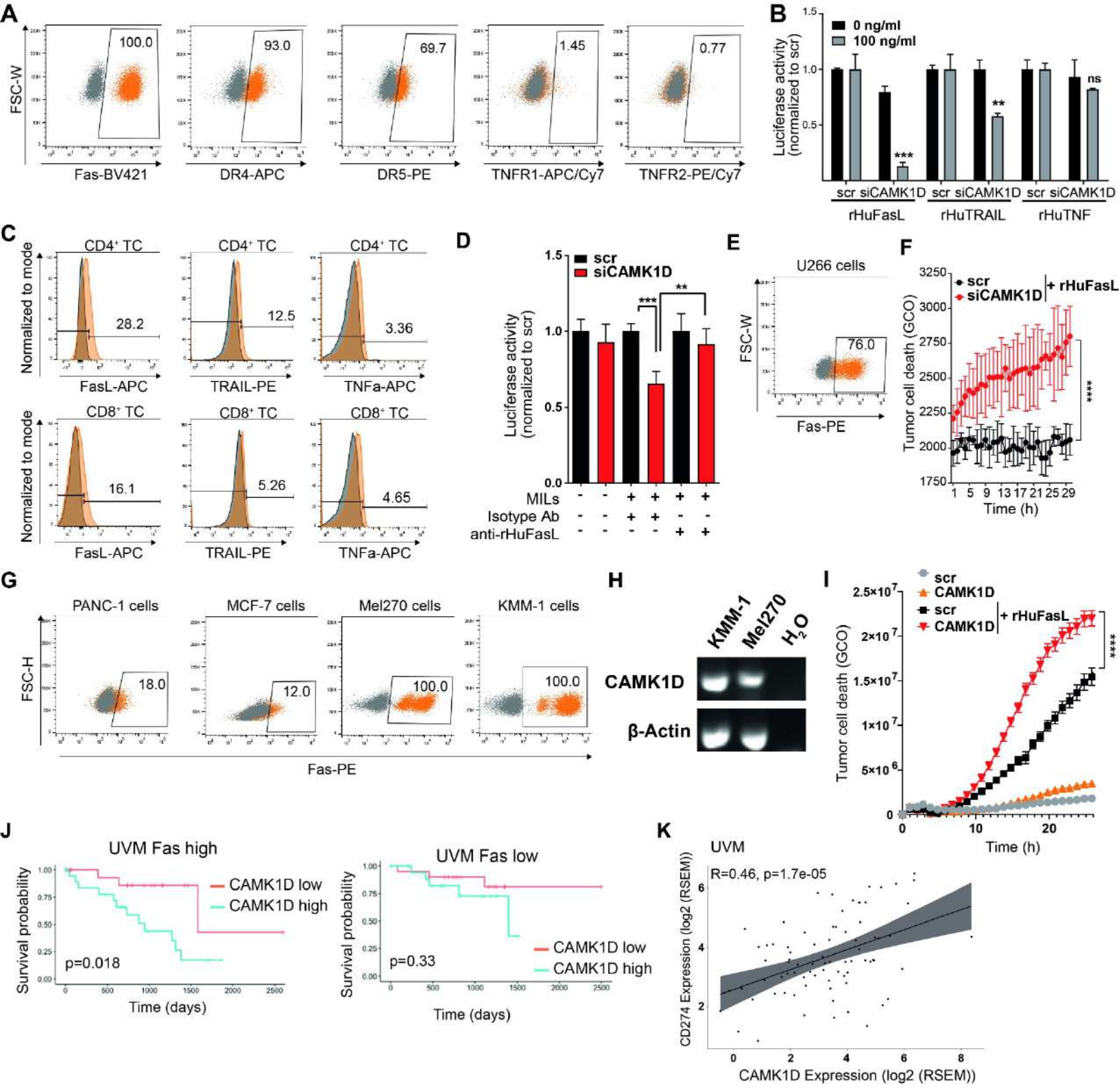
A
100.0
93.0
69.7
1.45
0.77
FSC-W
Fas-BV421
DR4-APC
DR5-PE
TNFR1-APC/Cy7
TNFR2-PE/Cy7
B
0 ng/ml
100 ng/ml
Luciferase activity (normalized to scr)
scr siCAMK1D scr siCAMK1D scr siCAMK1D
rHuFasL
rHuTRAIL
rHuTNF
ns
C
CD4+ TC
CD8+ TC
Normalized to mode
28.2
12.5
3.36
16.1
5.26
4.65
FasL-APC
TRAIL-PE
TNFa-APC
D
scr
siCAMK1D
Luciferase activity (normalized to scr)
MILs
Isotype Ab
anti-rHuFasL
E
U266 cells
76.0
FSC-W
Fas-PE
F
scr
siCAMK1D
+ rHuFasL
Tumor cell death (GCO)
Time (h)
G
PANC-1 cells
MCF-7 cells
Mel270 cells
KMM-1 cells
18.0
12.0
100.0
100.0
FSC-H
Fas-PE
H
KMM-1
Mel270
H2O
CAMK1D
β-Actin
I
scr
CAMK1D
scr
CAMK1D
+ rHuFasL
Tumor cell death (GCO)
Time (h)
J
UVM Fas high
CAMK1D low
CAMK1D high
p=0.018
Survival probability
Time (days)
UVM Fas low
CAMK1D low
CAMK1D high
p=0.33
Survival probability
Time (days)
K
UVM
R=0.46, p=1.7e-05
CD274 Expression (log2 (RSEM))
CAMK1D Expression (log2 (RSEM))

Figure 5

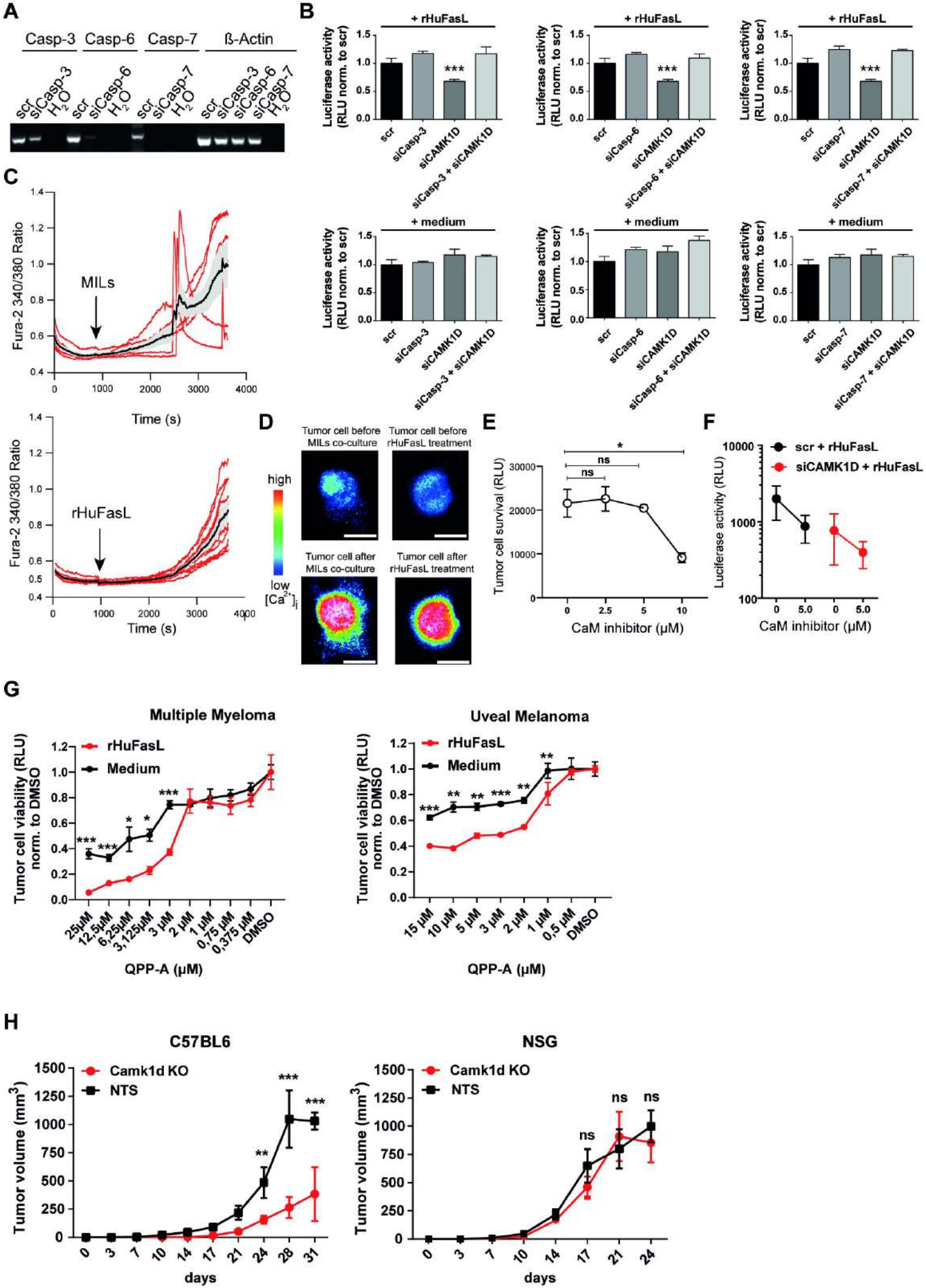
A
Casp-3
Casp-6
Casp-7
ß-Actin
scr
siCasp-3
siCasp-6
siCasp-7
H2O
B
+ rHuFasL
+ medium
Luciferase activity (RLU norm. to scr)
scr
siCasp-3
siCasp-6
siCasp-7
siCAMK1D
siCasp-3 + siCAMK1D
siCasp-6 + siCAMK1D
siCasp-7 + siCAMK1D
C
Fura-2 340/380 Ratio
MILs
rHuFasL
Time (s)
D
Tumor cell before MILs co-culture
Tumor cell before rHuFasL treatment
Tumor cell after MILs co-culture
Tumor cell after rHuFasL treatment
high
low
[Ca2+]i
E
Tumor cell survival (RLU)
CaM inhibitor (µM)
ns
*
F
scr + rHuFasL
siCAMK1D + rHuFasL
Luciferase activity (RLU)
CaM inhibitor (µM)
G
Multiple Myeloma
Uveal Melanoma
rHuFasL
Medium
Tumor cell viability (RLU) norm. to DMSO
QPP-A (µM)
25µM
12,5µM
6,25µM
3,125µM
3 µM
2 µM
1 µM
0,75 µM
0,375 µM
DMSO
15 µM
10 µM
5 µM
3 µM
2 µM
1 µM
0,5 µM
DMSO
H
C57BL6
NSG
Camk1d KO
NTS
Tumor volume (mm3)
days
ns

Figure 6

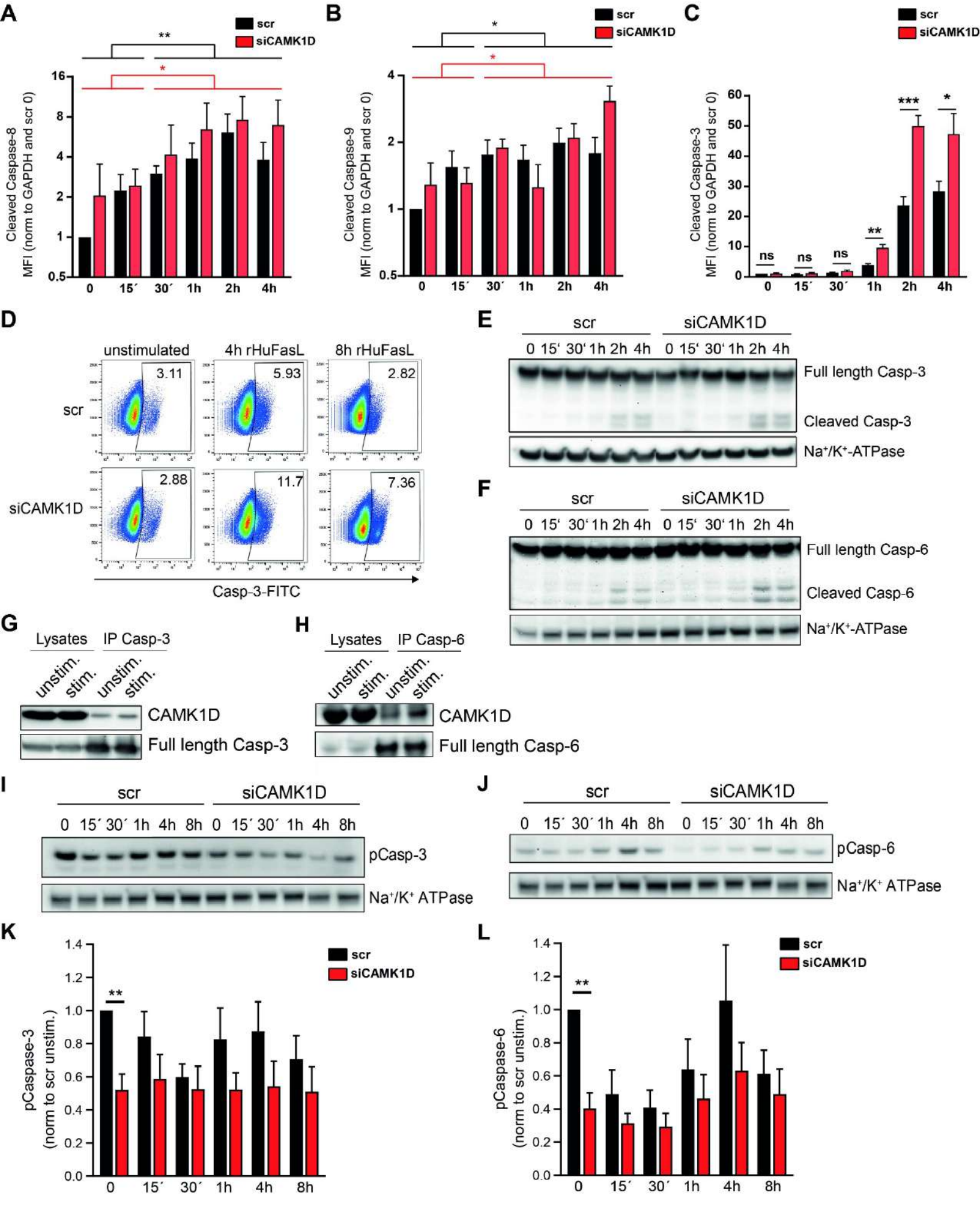
A
scr
siCAMK1D
Cleaved Caspase-8
MFI (norm to GAPDH and scr 0)
0 15´ 30´ 1h 2h 4h
B
Cleaved Caspase-9
MFI (norm to GAPDH and scr 0)
C
Cleaved Caspase-3
MFI (norm to GAPDH and scr 0)
ns
D
unstimulated
4h rHuFasL
8h rHuFasL
3.11
5.93
2.82
2.88
11.7
7.36
Casp-3-FITC
E
Full length Casp-3
Cleaved Casp-3
Na+/K+-ATPase
F
Full length Casp-6
Cleaved Casp-6
G
Lysates
IP Casp-3
unstim.
stim.
CAMK1D
Full length Casp-3
H
IP Casp-6
Full length Casp-6
I
pCasp-3
Na+/K+ ATPase
J
pCasp-6
K
pCaspase-3
(norm to scr unstim.)
L
pCaspase-6